

Latency Analysis for Sequential Detection in Low-Complexity Binary Radio Systems

Manuel S. Stein and Michael Fauß

Abstract

We consider the problem of making a quick decision in favor of one of two possible physical models while the numerical measurements are acquired by sensing devices featuring minimal digitization complexity. Therefore, the digital data streams available for statistical processing are binary and exhibit temporal and spatial dependencies. Such a setting is of relevance when designing radio systems that have to perform time-critical monitoring tasks in noisy environments with low energy consumption. We assess the latency penalty in sequential decision-making resulting from using analog-to-binary instead of high-resolution analog-to-digital conversion at the front-ends. To handle the intractable multivariate binary data model, we first consider sequential tests for exponential family distributions. Within this generic probabilistic framework, we identify approximations for the log-likelihood ratio and the Kullback–Leibler divergence. The results allow designing sequential detectors for binary radio systems and analyzing their average run-time along classical arguments of Wald. In particular, the derived tests exploit the structure of the spatio-temporal correlation of the analog sensor signals engraved into the binary radio data stream. As an application, we consider the specification of binary sensing architectures in the context of cognitive radio and satellite-based synchronization where our results characterize the detection latency as a function of the temporal oversampling and the number of antennas. Finally, we evaluate the efficiency of the proposed algorithms and illustrate the accuracy of our analysis via Monte-Carlo simulations.

Index Terms

array processing, cognitive radio, GNSS, Kullback-Leibler divergence, log-likelihood ratio, low complexity, low latency, quantization, radio front-end, sequential analysis, signal detection, spectrum monitoring, wireless systems, 1-bit ADC

M. S. Stein is with the Circuits and Systems Group, Technische Universiteit Delft, The Netherlands (e-mail: M.S.Stein@tudelft.nl). M. Fauß is with the Signal Processing Group, Technische Universität Darmstadt, Germany (e-mail: Michael.Fauss@spg.tu-darmstadt.de).

I. INTRODUCTION

The design of future sensor systems represents a challenge. For applications in the Internet of Things (IoT), the focus is on further miniaturization. Thus, small circuit size, low production cost, and low energy consumption are key requirements. In contrast, for safety-critical applications, sensing accuracy and detection reliability are of utmost importance. In any case, optimal system design either aims at achieving minimum complexity at a specified performance level, or at converting the available resources into maximum performance. Therefore, a thorough understanding of Pareto-optimal architectures is required, i.e., advanced sensor systems for which it is impossible to improve on complexity or performance without sacrificing the other measure.

A difficulty is that terms like complexity and performance are fuzzy without restriction to a specific perspective. In an R&D environment, the analog front-end engineers tend to equate complexity with the circuit area or the dissipated power, and performance with the degree of linearity. On the other hand, software engineers rather associate complexity with the computing effort and the size of the occupied memory, while performance is linked to the fast and correct response of the digital units to specific input data. In hardware-aware statistical signal processing, the understanding is emerging that a holistic approach is required when designing advanced sensor systems. In particular, this means that the physical phenomenon, the design of the analog front-end, and the digital processing need to be considered as a single joint problem.

For this purpose, it is helpful to reduce the system task to its fundamental building blocks. Elementary for sensing systems are parameter estimation and signal detection. While estimation aims at inferring data model parameters within an open set from noisy measurements, detection covers cases with discrete parameter space. To characterize performance, the accuracy in determining the parameters is central within estimation theory. Detection theory focuses on the reliability in discriminating between the possible models. An advantage of the parametric interpretation within these disciplines is that there is an understanding of optimal procedures. Also, analytic expressions are available to characterize the achievable accuracy or reliability. Hence, for optimal design in the above sense, it is desirable to formulate a suitable parametric probabilistic model as a function of the acquisition apparatus and the physical effects acting on it. Together with technology cost models, physical layouts can be determined which offer a favorable complexity-performance trade-off. Based on these considerations, system engineers can give detailed design recommendations to front-end engineers and software engineers.

A. Motivation

The purpose of this article is to highlight the opportunities and challenges of a hardware-aware system design approach. We limit ourselves to systems where the analog-to-digital (A/D) converters only forward the binary information concerning the sign of the analog sensor amplitude to the digital domain. The reasoning is that amplitude resolution increases A/D complexity exponentially. Each additional bit at least doubles the demand on A/D resources [1]. Thus, from a complexity-aware perspective, digitization with more than 1-bit amplitude resolution appears unfavorable, in particular, when most bits represent uninformative noise. Furthermore, binary digitization has beneficial effects on low-level processing, where the resulting data can be handled with low complexity. However, such savings are obtained by accepting a considerable loss of information during signal acquisition. A thorough analysis, however, shows that probabilistic modeling of the transition from a physical phenomenon to binary measurements, front-end optimization and the use of likelihood-oriented processing techniques can largely compensate for the effect of digitization-induced distortion on the final inference solution, see, e.g., [2]. While binary sampling has been extensively studied, e.g., with respect to wireless communication capabilities [3]–[8], signal reconstruction error [9]–[11], estimation sensitivity [12]–[17] and detection reliability [18]–[20], here we focus on the analysis of the sensing latency [21].

The binary data stream is assumed to be processed in short spatio-temporal blocks with the goal to quickly detect which of two physical scenarios is generating the measurements. The reliability to be achieved is predetermined. Leaning on concepts from sequential analysis [22], [23], we characterize the average sampling number required for reliable detection when binary sensors are employed. A fundamental challenge which we address is the fact that the probabilistic models characterizing multivariate binary measurements are, in general, intractable [24]. A workaround, aiming at approximating likelihood-based sequential testing, enables analyzing the detection latency as a function of the binary sensing architecture and the two underlying physical models.

The article outlines applications related to mobile radio communication and satellite-based synchronization systems. On the one hand, we consider cognitive radio where a secondary user observes the activity of a primary user [25]. Once the primary wireless transmitter is inactive, the secondary system uses the communication channel. Thus, without limiting the functionality of the primary user or occupying additional bands, spectral resources can be used for wireless services. Since mobile radio systems necessitate a cost-efficient and miniaturized

design, reliable operation at low complexity is crucial. On the other hand, we treat monitoring of safety-critical satellite-radio frequencies [26]. Due to the low power and the distance of the global navigation satellite system (GNSS) transmitters, terrestrial radio interference poses a challenge. Small jamming devices, which protect the privacy of individuals, can impair the functionality of critical infrastructure (e.g., financial markets, power network, airports, communication networks), which ensures the safety and well-being of many people [27]. For monitoring the GNSS spectrum in the vicinity of safety-critical receivers, high sensing performance is of utmost importance.

Both applications have in common that during system development a favorable complexity-performance trade-off has to be identified. In addition to reaching reliability, minimizing latency plays a decisive role. A cognitive system with small decision delay enables using spectral resources efficiently. A monitoring receiver which quickly detects interference can initiate measures for suppression or declare malfunctioning in time. For such architectures, we perform hardware-aware modeling of the analog front-ends and the resulting binary measurements. Our analytic findings characterize how the temporal oversampling and the number of sensors affect the sequential detection latency. Additionally, we use A/D cost models to identify cases in which it is advantageous to consider designs with higher resolution. We close the academic discourse by evaluating the developed sequential algorithms and illustrating the accuracy of our latency analysis utilizing synthetically generated data streams from exemplary binary radio systems.

B. Related Work

Quantized sequential decision-making has been studied predominantly for sensor networks where measurement nodes forward compressed statistics of their observations to minimize the communication overhead [28]–[34]. In such a setup, it is usually assumed that the nodes have access to the unquantized observations and compress them, for example, by quantizing the likelihood ratio. Here we discuss sequential detection when employing binary sensing front-ends. Therefore, the nodes do not have access to the high-resolution observations, and the central decision is exclusively based on hard-limited measurements. This case is less well studied, and the focus of existing works is on the design of optimal quantizer design [21], [35]–[37].

C. Contribution

In contrast, we consider quantizers of minimal complexity. Therefore, the analog signals are converted into binary data by symmetric hard-limiting. Furthermore, we assume random signals

with temporal and spatial dependencies. Sequential analysis then exhibits particular challenges and, to the best of our knowledge, has not been discussed yet. Due to the highly nonlinear signal acquisition, one cannot rely on linear system theory and Gaussian statistics when modeling the sensor data. Such methods only provide good results when a sufficiently high A/D resolution is deployed. On the other hand, with exact approaches, see, e.g., [38]–[40], the analysis becomes difficult, when considering correlation at the hard-limiter input. For the resulting multivariate binary data, the probability mass function and the sufficient statistics grow exponentially with the number of dimensions [41]. Furthermore, the unknown orthant probabilities [42] with more than four variables (open problem in mathematics) hinders access to the likelihood. We address this by exploiting properties of the exponential family. Such a probabilistic perspective onto hardware-aware signal processing systems [24] provides an approximate log-likelihood ratio (ALLR) and, therefore, enables performing a sequential probability ratio test (SPRT) for a broad class of data models without access to the exact likelihood ratio. Additionally, the approach provides approximations for the Kullback–Leibler divergence characterizing the average sampling number (ASN) of the approximate SPRT (ASPR). Further, using an auxiliary exponential distribution of reduced statistical complexity, we ensure computational tractability. Studying the efficiency of binary sensor layouts via the analytic results, we show that with temporal and spatial oversampling, it is possible to perform challenging sequential tasks reliably. In particular, the possibility to deploy more antennas enables sensing with a superior complexity-performance trade-off. Note that this article is an extension of our special session contribution [43].

II. PROBLEM FORMULATION

A. System Model - Signal Acquisition

We consider $M \in \mathbb{N}$ analog sensor outputs, modeled as real-valued time-continuous functions

$$\mathbf{y}(t) = \mathbf{s}(t) + \boldsymbol{\eta}(t). \quad (1)$$

The outputs $\mathbf{y}(t) \in \mathbb{R}^M$, $t \in \mathbb{R}$, are the superposition of a source component $\mathbf{s}(t) \in \mathbb{R}^M$ and additive independent measurement noise $\boldsymbol{\eta}(t) \in \mathbb{R}^M$. Both signals are modeled as band-limited wide-sense stationary Gaussian processes with zero mean. The M analog output signals (1) are synchronously discretized in batches of K equidistant points in time. With infinite digital amplitude resolution, the n th observation instance provides a space-time sample

$$\mathbf{y}_n = \left[\mathbf{y}_n^T[1] \quad \mathbf{y}_n^T[2] \quad \dots \quad \mathbf{y}_n^T[K] \right]^T \in \mathbb{R}^{MK}, \quad (2)$$

where, with the sampling interval $T \in \mathbb{R}$, we write

$$\mathbf{y}_n[k] = \mathbf{y}((n-1)KT + (k-1)T), \quad k = 1, \dots, K. \quad (3)$$

Note, that the sampling duration for each block (2) is $T_o = KT$. We consider the dependencies between consecutive space-time samples as negligible, such that for each n (2) can be considered independent. Due to stationarity and Gaussianity in (1), the spatio-temporal data (2) follows

$$\mathbf{y} = \mathbf{s} + \boldsymbol{\eta} \quad \text{and} \quad \mathbf{y} \sim \mathcal{N}(\mathbf{0}, \mathbf{R}_y(\boldsymbol{\theta})), \quad (4)$$

where the space-time covariance matrix

$$\mathbf{R}_y(\boldsymbol{\theta}) = \mathbb{E}_{\mathbf{y};\boldsymbol{\theta}} [\mathbf{y}\mathbf{y}^T] = \mathbf{R}_s(\boldsymbol{\theta}) + \mathbf{R}_\eta \in \mathbb{R}^{MK \times MK} \quad (5)$$

is a superposition of the source $\mathbf{R}_s(\boldsymbol{\theta}) = \mathbb{E}_{\mathbf{s};\boldsymbol{\theta}} [\mathbf{s}\mathbf{s}^T]$ and the noise covariance $\mathbf{R}_\eta = \mathbb{E}_\eta [\boldsymbol{\eta}\boldsymbol{\eta}^T]$. The source covariance is a function of parameters $\boldsymbol{\theta} \in \mathbb{R}^D$, while the noise covariance is constant.

Realizing a signal acquisition which approximately produces a data stream according to the multivariate Gaussian model (4), in practice, requires an A/D converter with several bits digital amplitude resolution at each analog output. To minimize A/D complexity, we here assume that within the considered system only the signs of the analog measurements $\mathbf{y}(t)$ are transferred to the digital domain. Such a binary signal acquisition results in the space-time observations

$$\mathbf{z}_n = \text{sign}(\mathbf{y}_n), \quad (6)$$

where the element-wise symmetric hard-limiter $\text{sign}(\cdot)$ is defined such that

$$[\mathbf{z}_n]_i = \begin{cases} +1 & \text{if } [\mathbf{y}_n]_i \geq 0, \\ -1 & \text{if } [\mathbf{y}_n]_i < 0. \end{cases} \quad (7)$$

Per space-time sample (2), analog-to-binary (A/B) conversion (6) can be realized by K comparator operations for each of the M analog outputs, while a b -bit receiver requires to activate

$$\text{SC}^{(b)}(M, K) = MK(2^b - 1) \quad (8)$$

comparators. Further, the binary data (6) can be stored on small memory, transmitted using channels with moderate capacity, and processed at high rate and low computational cost.

B. Processing Task - Sequential Decision-Making

The binary measurements (6) gathered up to the n th observation instance, are summarized

$$\mathbf{Z}_n = \begin{bmatrix} z_1 & z_2 & \dots & z_n \end{bmatrix}, \quad \mathbf{Z}_n \in \mathbb{B}^{MK \times n}. \quad (9)$$

The inference task is to use the available data \mathbf{Z}_n to decide which of the two probability laws

$$\mathcal{H}_0: \mathbf{z} \sim p_{\mathbf{z}}(\mathbf{z}; \boldsymbol{\theta}_0) \quad \text{or} \quad \mathcal{H}_1: \mathbf{z} \sim p_{\mathbf{z}}(\mathbf{z}; \boldsymbol{\theta}_1) \quad (10)$$

is the model generating the output (6). The detection is to be conducted reliably, i.e.,

$$\Pr \{\text{decision } \mathcal{H}_0 | \mathcal{H}_1\} \leq \alpha_0 \quad \text{and} \quad \Pr \{\text{decision } \mathcal{H}_1 | \mathcal{H}_0\} \leq \alpha_1. \quad (11)$$

If a decision based on \mathbf{Z}_n would lead to a violation of the reliability constraints, the processing unit waits for the next space-time sample z_{n+1} and tries to perform the test with the augmented data stream \mathbf{Z}_{n+1} . The instance in which the detection is finally performed is denoted by n_{D} . The performance of the sequential test is characterized by the average sampling number (ASN), which is defined as the expected value of n_{D} under the data-generating model $p_{\mathbf{z}}(\mathbf{z}; \boldsymbol{\theta})$, i.e.,

$$\text{ASN}(\boldsymbol{\theta}) = \mathbb{E}_{n_{\text{D}}; \boldsymbol{\theta}} [n_{\text{D}}]. \quad (12)$$

A classical approach to construct such a low-latency decision-making algorithm is the sequential probability ratio test (SPRT) [22]. Given the data stream \mathbf{Z}_n , the log-likelihood ratio (LLR)

$$l(\mathbf{Z}_n) = \sum_{i=1}^n l(z_i) = \sum_{i=1}^n \ln \frac{p_{\mathbf{z}}(z_n; \boldsymbol{\theta}_1)}{p_{\mathbf{z}}(z_n; \boldsymbol{\theta}_0)} \quad (13)$$

is calculated and compared against two decision thresholds. If

$$l(\mathbf{Z}_n) \leq \ln \frac{\alpha_1}{1 - \alpha_0} = L_0, \quad (14)$$

the test is stopped with a decision in favor of \mathcal{H}_0 . In case

$$l(\mathbf{Z}_n) \geq \ln \frac{1 - \alpha_1}{\alpha_0} = L_1, \quad (15)$$

the sequential test is terminated in favor of the hypothesis \mathcal{H}_1 . Otherwise, an additional signal sample z_{n+1} is taken to continue the test with \mathbf{Z}_{n+1} . With the short notations

$$\begin{aligned} N_0 &= (1 - \alpha_0) \ln \frac{\alpha_1}{1 - \alpha_0} + \alpha_0 \ln \frac{1 - \alpha_1}{\alpha_0}, \\ N_1 &= \alpha_1 \ln \frac{\alpha_1}{1 - \alpha_0} + (1 - \alpha_1) \ln \frac{1 - \alpha_1}{\alpha_0}, \end{aligned} \quad (16)$$

the ASN of the SPRT under the two possible data model hypotheses (10) is approximately [22]

$$\text{ASN}_0 \approx \frac{N_0}{\mathbb{E}_{\mathbf{z};\boldsymbol{\theta}_0} [l(\mathbf{z})]} = -\frac{N_0}{D(p_{\mathbf{z};\boldsymbol{\theta}_0} || p_{\mathbf{z};\boldsymbol{\theta}_1})} \quad (17)$$

and

$$\text{ASN}_1 \approx \frac{N_1}{\mathbb{E}_{\mathbf{z};\boldsymbol{\theta}_1} [l(\mathbf{z})]} = \frac{N_1}{D(p_{\mathbf{z};\boldsymbol{\theta}_1} || p_{\mathbf{z};\boldsymbol{\theta}_0})}, \quad (18)$$

where $D(p_{\mathbf{u};\boldsymbol{\theta}} || q_{\mathbf{w};\boldsymbol{\theta}})$ denotes the Kullback–Leibler divergence between $p_{\mathbf{u}}(\mathbf{u}; \boldsymbol{\theta})$ and $q_{\mathbf{w}}(\mathbf{w}; \boldsymbol{\theta})$.

C. Challenge - Data Models for Binary Measurements

While A/B conversion according to (6) offers significant savings regarding hardware cost and power consumption, the probabilistic characterization of the binary sensor outputs forms a challenge. To obtain the exact binary likelihood required in (13), the multidimensional integral

$$p_{\mathbf{z}}(\mathbf{z}; \boldsymbol{\theta}) = \int_{\mathcal{Y}(\mathbf{z})} p_{\mathbf{y}}(\mathbf{y}; \boldsymbol{\theta}) d\mathbf{y} \quad (19)$$

needs to be evaluated, where $p_{\mathbf{y}}(\mathbf{y}; \boldsymbol{\theta})$ denotes the parametric input distribution to (6) and

$$\mathcal{Y}(\mathbf{z}) = \{\mathbf{y} \in \mathbb{R}^{MK} \mid \mathbf{z} = \text{sign}(\mathbf{y})\}. \quad (20)$$

The exact calculation of an integral like (19) can turn out to be challenging. If, like in our case, the input to the quantizer (6) is zero-mean multivariate Gaussian, evaluation of (19) requires the orthant probability, for which general expressions are only known for cases with $MK \leq 4$. Even if analytic solutions for (19) were available, the memory required to store all possible values for a single hypothesis scales as $\mathcal{O}(2^{MK})$. This renders using (13) and analyzing the resulting ASN by (17) and (18) prohibitively complex even for scenarios with moderately large M and K .

III. LIKELIHOOD RATIO IN THE EXPONENTIAL FAMILY

A conceptual observation which turns out useful is that the distribution of the multivariate binary measurements (6) can be modeled within the framework of the exponential family [24].

A. Exponential Family Data Models

A distribution belongs to the exponential family if it factorizes as

$$p_{\mathbf{u}}(\mathbf{u}; \boldsymbol{\theta}) = \exp(\boldsymbol{\beta}^T(\boldsymbol{\theta})\boldsymbol{\phi}(\mathbf{u}) - \lambda(\boldsymbol{\theta}) + \nu(\mathbf{u})), \quad (21)$$

where we call $\mathbf{u} \in \mathcal{U}$ the V -dimensional multivariate random variable with support \mathcal{U} , $\boldsymbol{\theta} \in \mathbb{R}^D$ the physical parameters, $\boldsymbol{\beta}(\boldsymbol{\theta}): \mathbb{R}^D \rightarrow \mathbb{R}^C$ the statistical parameters, $\boldsymbol{\phi}(\mathbf{u}): \mathcal{U}^V \rightarrow \mathbb{R}^C$ the sufficient statistics, $\lambda(\boldsymbol{\theta}): \mathbb{R}^D \rightarrow \mathbb{R}$ the log-normalizer and $\nu(\mathbf{u}): \mathcal{U} \rightarrow \mathbb{R}$ the carrier measure. We use this particular denomination for the components of (21) to emphasize that, in our engineering-oriented perspective, a probabilistic data model $p_{\mathbf{u}}(\mathbf{u}; \boldsymbol{\theta})$ characterizes a connection between the physical phenomenon $\boldsymbol{\theta}$ and digital data \mathbf{u} . While the multivariate Gaussian model (4) also factorizes according to (21), the number of its sufficient statistics C scales as $\mathcal{O}(V^2)$. For a multivariate binary model, in contrast, the sufficient statistics scale as $\mathcal{O}(2^V)$ [41]. Therefore,

$$l(\mathbf{z}) = \ln \frac{p_{\mathbf{z}}(\mathbf{z}; \boldsymbol{\theta}_1)}{p_{\mathbf{z}}(\mathbf{z}; \boldsymbol{\theta}_0)}, \quad (22)$$

required in (13), is inconvenient to handle. In the following, we discuss an approximation $\tilde{l}(\mathbf{z}) \approx l(\mathbf{z})$, enabling to implement the test defined in (13)–(15) and assess its latency (17) and (18) via

$$\mathbb{E}_{\mathbf{z}; \boldsymbol{\theta}_i} [l(\mathbf{z})] \approx \mathbb{E}_{\mathbf{z}; \boldsymbol{\theta}_i} [\tilde{l}(\mathbf{z})], \quad i = 1, 2. \quad (23)$$

Note that a tractable expression on the right-hand of (23) which is sufficiently close to the left-hand side, implies a relevant approximation for the Kullback–Leibler divergence.

The LLR between two different hypotheses within the framework (21) is given by

$$l(\mathbf{u}) = (\boldsymbol{\beta}(\boldsymbol{\theta}_1) - \boldsymbol{\beta}(\boldsymbol{\theta}_0))^{\text{T}} \boldsymbol{\phi}(\mathbf{u}) - (\lambda(\boldsymbol{\theta}_1) - \lambda(\boldsymbol{\theta}_0)), \quad (24)$$

such that, with the mean of the sufficient statistics

$$\boldsymbol{\mu}_{\boldsymbol{\phi}}(\boldsymbol{\theta}) = \mathbb{E}_{\mathbf{u}; \boldsymbol{\theta}} [\boldsymbol{\phi}(\mathbf{u})] \quad (25)$$

and their covariance matrix

$$\mathbf{R}_{\boldsymbol{\phi}}(\boldsymbol{\theta}) = \mathbb{E}_{\mathbf{u}; \boldsymbol{\theta}} \left[(\boldsymbol{\phi}(\mathbf{u}) - \boldsymbol{\mu}_{\boldsymbol{\phi}}(\boldsymbol{\theta})) (\boldsymbol{\phi}(\mathbf{u}) - \boldsymbol{\mu}_{\boldsymbol{\phi}}(\boldsymbol{\theta}))^{\text{T}} \right], \quad (26)$$

the mean of the LLR is given by

$$\mu_i = \mathbb{E}_{\mathbf{z}; \boldsymbol{\theta}_i} [l(\mathbf{z})] = (\boldsymbol{\beta}(\boldsymbol{\theta}_1) - \boldsymbol{\beta}(\boldsymbol{\theta}_0))^{\text{T}} \boldsymbol{\mu}_{\boldsymbol{\phi}}(\boldsymbol{\theta}_i) - (\lambda(\boldsymbol{\theta}_1) - \lambda(\boldsymbol{\theta}_0)), \quad (27)$$

while the variance of the LLR can be written as

$$\sigma_i^2 = \mathbb{E}_{\mathbf{z}; \boldsymbol{\theta}_i} \left[(l(\mathbf{z}) - \mathbb{E}_{\mathbf{z}; \boldsymbol{\theta}_i} [l(\mathbf{z})])^2 \right] = (\boldsymbol{\beta}(\boldsymbol{\theta}_1) - \boldsymbol{\beta}(\boldsymbol{\theta}_0))^{\text{T}} \mathbf{R}_{\boldsymbol{\phi}}(\boldsymbol{\theta}_i) (\boldsymbol{\beta}(\boldsymbol{\theta}_1) - \boldsymbol{\beta}(\boldsymbol{\theta}_0)). \quad (28)$$

B. Approximations for the Exponential Family LLR

In practice, access to the statistical parameters $\beta(\boldsymbol{\theta})$ and the log-normalizer $\lambda(\boldsymbol{\theta})$, for executing and analyzing likelihood-based tests, can be difficult to obtain. For example, for the output (6)

$$\lambda(\boldsymbol{\theta}) = \ln \int_{\mathcal{U}} \exp(\boldsymbol{\beta}^T(\boldsymbol{\theta})\boldsymbol{\phi}(\mathbf{u}) + \nu(\mathbf{u})) d\mathbf{u} \quad (29)$$

results in a sum with 2^{MK} terms. To obtain a representation of (24) which does not require explicit access to $\beta(\boldsymbol{\theta})$ and $\lambda(\boldsymbol{\theta})$, we assume to have at hand (25) and (26) as function of $\boldsymbol{\theta}$. These measures are usually easier to obtain than $\beta(\boldsymbol{\theta})$ and $\lambda(\boldsymbol{\theta})$. To link (25) and (26) to the exponential family LLR (24), we use that all distributions (21) exhibit regularity, i.e.,

$$\mathbb{E}_{\mathbf{u};\boldsymbol{\theta}} \left[\frac{\partial \ln p_{\mathbf{u}}(\mathbf{u}; \boldsymbol{\theta})}{\partial \boldsymbol{\theta}} \right] = \mathbf{0}^T. \quad (30)$$

Therefore, for any exponential family (21), it holds that

$$\left(\frac{\partial \lambda(\boldsymbol{\theta})}{\partial \boldsymbol{\theta}} \right)^T = \left(\frac{\partial \beta(\boldsymbol{\theta})}{\partial \boldsymbol{\theta}} \right)^T \boldsymbol{\mu}_{\phi}(\boldsymbol{\theta}). \quad (31)$$

Defining an LLR linearization point

$$\tilde{\boldsymbol{\theta}}(\xi) = \xi \boldsymbol{\theta}_0 + (1 - \xi) \boldsymbol{\theta}_1, \quad \xi \in [0, 1], \quad (32)$$

and applying the finite difference approximation (108) in the Appendix together with the regularity constraint (31), we obtain

$$\lambda(\boldsymbol{\theta}_1) - \lambda(\boldsymbol{\theta}_0) \approx \frac{\partial \lambda(\tilde{\boldsymbol{\theta}}(\xi))}{\partial \boldsymbol{\theta}} (\boldsymbol{\theta}_1 - \boldsymbol{\theta}_0) = \boldsymbol{\mu}_{\phi}^T(\tilde{\boldsymbol{\theta}}(\xi)) \frac{\partial \beta(\tilde{\boldsymbol{\theta}}(\xi))}{\partial \boldsymbol{\theta}} (\boldsymbol{\theta}_1 - \boldsymbol{\theta}_0). \quad (33)$$

Further, for all distributions in the exponential family (21), one has [24]

$$\frac{\partial \beta(\boldsymbol{\theta})}{\partial \boldsymbol{\theta}} = \mathbf{R}_{\phi}^{-1}(\boldsymbol{\theta}) \frac{\partial \boldsymbol{\mu}_{\phi}(\boldsymbol{\theta})}{\partial \boldsymbol{\theta}}, \quad (34)$$

such that (33) can be reformulated as

$$\lambda(\boldsymbol{\theta}_1) - \lambda(\boldsymbol{\theta}_0) \approx \boldsymbol{\mu}_{\phi}^T(\tilde{\boldsymbol{\theta}}(\xi)) \mathbf{R}_{\phi}^{-1}(\tilde{\boldsymbol{\theta}}(\xi)) \frac{\partial \boldsymbol{\mu}_{\phi}(\tilde{\boldsymbol{\theta}}(\xi))}{\partial \boldsymbol{\theta}} (\boldsymbol{\theta}_1 - \boldsymbol{\theta}_0). \quad (35)$$

Accordingly, the difference of the statistical parameters in (24) is approximated by

$$\beta(\boldsymbol{\theta}_1) - \beta(\boldsymbol{\theta}_0) \approx \frac{\partial \beta(\tilde{\boldsymbol{\theta}}(\xi))}{\partial \boldsymbol{\theta}} (\boldsymbol{\theta}_1 - \boldsymbol{\theta}_0) = \mathbf{R}_{\phi}^{-1}(\tilde{\boldsymbol{\theta}}(\xi)) \frac{\partial \boldsymbol{\mu}_{\phi}(\tilde{\boldsymbol{\theta}}(\xi))}{\partial \boldsymbol{\theta}} (\boldsymbol{\theta}_1 - \boldsymbol{\theta}_0). \quad (36)$$

With the definition of an LLR hyperplane

$$\mathbf{b}_{\partial}(\boldsymbol{\theta}_0, \boldsymbol{\theta}_1; \xi) = \mathbf{R}_{\phi}^{-1}(\tilde{\boldsymbol{\theta}}(\xi)) \frac{\partial \boldsymbol{\mu}_{\phi}(\tilde{\boldsymbol{\theta}}(\xi))}{\partial \boldsymbol{\theta}} (\boldsymbol{\theta}_1 - \boldsymbol{\theta}_0), \quad (37)$$

and using (35) and (36) in (24), we obtain a first approximation for (24) by the expression

$$l(\mathbf{u}) \approx \mathbf{b}_\theta^\top(\boldsymbol{\theta}_0, \boldsymbol{\theta}_1; \xi) \left(\boldsymbol{\phi}(\mathbf{u}) - \boldsymbol{\mu}_\phi(\tilde{\boldsymbol{\theta}}(\xi)) \right) = \tilde{l}_\theta(\mathbf{u}; \xi). \quad (38)$$

The structure of the approximation (38) enables interpreting the LLR in exponential families as the signed distance of a sufficient statistics residual from the hyperplane (37). Note, that (37) requires access to the derivative of (25) with respect to $\boldsymbol{\theta}$ evaluated at $\tilde{\boldsymbol{\theta}}(\xi)$. Using the finite difference (108) to eliminate the derivative in (37), the LLR hyperplane can also be written as

$$\mathbf{b}(\boldsymbol{\theta}_0, \boldsymbol{\theta}_1; \xi) = \mathbf{R}_\phi^{-1}(\tilde{\boldsymbol{\theta}}(\xi)) (\boldsymbol{\mu}_\phi(\boldsymbol{\theta}_1) - \boldsymbol{\mu}_\phi(\boldsymbol{\theta}_0)). \quad (39)$$

Therefore, an alternative to the exponential family LLR approximation (38) is

$$l(\mathbf{u}) \approx \mathbf{b}^\top(\boldsymbol{\theta}_0, \boldsymbol{\theta}_1; \xi) \left(\boldsymbol{\phi}(\mathbf{u}) - \boldsymbol{\mu}_\phi(\tilde{\boldsymbol{\theta}}(\xi)) \right) = \tilde{l}(\mathbf{u}; \xi). \quad (40)$$

Evaluating (40) requires access to (25) with respect to $p_u(\mathbf{u}; \boldsymbol{\theta}_0)$, $p_u(\mathbf{u}; \boldsymbol{\theta}_1)$, and $p_u(\mathbf{u}; \tilde{\boldsymbol{\theta}}(\xi))$. Further, one requires (26) with respect to $p_u(\mathbf{u}; \tilde{\boldsymbol{\theta}}(\xi))$. The integrals (19) or (29) are not required.

IV. APPROXIMATE TESTS IN THE EXPONENTIAL FAMILY

A. Approximate Sequential Probability Ratio Test

Defining the empirical mean of the statistics, computed from data \mathbf{U} with N columns, by

$$\hat{\boldsymbol{\phi}}(\mathbf{U}) = \frac{1}{N} \sum_{i=1}^N \boldsymbol{\phi}(\mathbf{u}_i), \quad (41)$$

and using one of the LLR approximations (38) or (40), for any data stream associated with a probabilistic model (21), an approximate SPRT (ASPRT) can be performed by comparing

$$\tilde{l}_\theta(\mathbf{U}_n; \xi) = \sum_{i=1}^n \tilde{l}_\theta(\mathbf{u}_i; \xi) = n \mathbf{b}_\theta^\top(\boldsymbol{\theta}_0, \boldsymbol{\theta}_1; \xi) (\hat{\boldsymbol{\phi}}(\mathbf{U}_n) - \tilde{\boldsymbol{\mu}}_\phi(\xi)) \quad (42)$$

or

$$\tilde{l}(\mathbf{U}_n; \xi) = n \mathbf{b}^\top(\boldsymbol{\theta}_0, \boldsymbol{\theta}_1; \xi) (\hat{\boldsymbol{\phi}}(\mathbf{U}_n) - \tilde{\boldsymbol{\mu}}_\phi(\xi)), \quad (43)$$

to the decision thresholds (14) and (15). The latency (12) of such a sequential detection algorithm can be assessed using (17) and (18) with the mean of the approximate LLR (ALLR)

$$\tilde{\mu}_{\theta,i}(\xi) = \mathbb{E}_{\mathbf{u}; \boldsymbol{\theta}_i} [\tilde{l}_\theta(\mathbf{u}; \xi)] = \mathbf{b}_\theta^\top(\boldsymbol{\theta}_0, \boldsymbol{\theta}_1; \xi) (\boldsymbol{\mu}_\phi(\boldsymbol{\theta}_i) - \tilde{\boldsymbol{\mu}}_\phi(\xi)), \quad i = 1, 2, \quad (44)$$

or

$$\tilde{\mu}_i(\xi) = \mathbf{b}^\top(\boldsymbol{\theta}_0, \boldsymbol{\theta}_1; \xi) (\boldsymbol{\mu}_\phi(\boldsymbol{\theta}_i) - \tilde{\boldsymbol{\mu}}_\phi(\xi)), \quad i = 1, 2. \quad (45)$$

Further, the analytic variance of the ALLR is

$$\tilde{\sigma}_{\partial,i}^2(\xi) = \mathbb{E}_{\mathbf{u};\boldsymbol{\theta}_i} \left[\left(\tilde{l}_{\partial}(\mathbf{u}; \xi) - \tilde{\mu}_{\partial,i}(\xi) \right)^2 \right] = \mathbf{b}_{\partial}^{\text{T}}(\boldsymbol{\theta}_0, \boldsymbol{\theta}_1; \xi) \mathbf{R}_{\phi}(\boldsymbol{\theta}_i) \mathbf{b}_{\partial}(\boldsymbol{\theta}_0, \boldsymbol{\theta}_1; \xi), \quad i = 1, 2, \quad (46)$$

or

$$\tilde{\sigma}_i^2(\xi) = \mathbf{b}^{\text{T}}(\boldsymbol{\theta}_0, \boldsymbol{\theta}_1; \xi) \mathbf{R}_{\phi}(\boldsymbol{\theta}_i) \mathbf{b}(\boldsymbol{\theta}_0, \boldsymbol{\theta}_1; \xi), \quad i = 1, 2. \quad (47)$$

B. Tuning of the Log-Likelihood Ratio Linearization Model

Obviously, the choice of the probabilistic linearization model $p_{\mathbf{u}}(\mathbf{u}; \tilde{\boldsymbol{\theta}}(\xi))$ via ξ impacts the accuracy of (38) and (40). While one can use $\xi = \frac{1}{2}$, we propose a heuristic method to adapt ξ . The idea is as follows: Instead of using the *geometric* midpoint between $\boldsymbol{\theta}_0$ and $\boldsymbol{\theta}_1$, we use the *statistical* midpoint. That is, we tune ξ such that the approximated test statistic $\tilde{l}(\mathbf{u})$ admits the same properties under both hypotheses. More precisely, we consider the standardized drift

$$\tilde{d}_i(\xi) = \frac{|\tilde{\mu}_i(\xi)|}{\tilde{\sigma}_i^{\rho}(\xi)}, \quad i = 0, 1, \quad (48)$$

where $\rho > 0$ can be chosen freely. Note that (48) is closely related to the error probabilities of the underlying test: for $d_i = 0$, the test does not admit a drift towards any threshold such that it decides randomly; for $d_i \rightarrow \infty$, the mean of the LLR dominates the variance making the test decide correctly for \mathcal{H}_i with probability one. To balance the decision-making performances under both hypotheses, it needs to hold that $\tilde{d}_1(\xi) \approx \tilde{d}_0(\xi)$. Therefore, we define the ratio

$$\tilde{\nu}(\xi) = \frac{|\tilde{\mu}_1(\xi)| \tilde{\sigma}_0^{\rho}(\xi)}{|\tilde{\mu}_0(\xi)| \tilde{\sigma}_1^{\rho}(\xi)} \quad (49)$$

and choose the linearization parameter ξ such that the difference between the drifts is minimized

$$\xi^* = \arg \min_{\xi \in [0;1]} (\tilde{\nu}(\xi) - 1)^2. \quad (50)$$

This approach results in sufficiently close approximations, as illustrated by examples in Sec. V.

C. Approximations for the Kullback–Leibler Divergence

Within (21), the results (44) and (45) imply approximations for Kullback–Leibler divergence

$$D(p_{\mathbf{u};\boldsymbol{\theta}_0} \| p_{\mathbf{u};\boldsymbol{\theta}_1}) \approx -(\boldsymbol{\theta}_1 - \boldsymbol{\theta}_0)^{\text{T}} \left(\frac{\partial \boldsymbol{\mu}_{\phi}(\tilde{\boldsymbol{\theta}}(\xi))}{\partial \boldsymbol{\theta}} \right)^{\text{T}} \mathbf{R}_{\phi}^{-1}(\tilde{\boldsymbol{\theta}}(\xi)) (\boldsymbol{\mu}_{\phi}(\boldsymbol{\theta}_0) - \tilde{\boldsymbol{\mu}}_{\phi}(\xi)), \quad (51)$$

$$D(p_{\mathbf{u};\boldsymbol{\theta}_1} \| p_{\mathbf{u};\boldsymbol{\theta}_0}) \approx (\boldsymbol{\theta}_1 - \boldsymbol{\theta}_0)^{\text{T}} \left(\frac{\partial \boldsymbol{\mu}_{\phi}(\tilde{\boldsymbol{\theta}}(\xi))}{\partial \boldsymbol{\theta}} \right)^{\text{T}} \mathbf{R}_{\phi}^{-1}(\tilde{\boldsymbol{\theta}}(\xi)) (\boldsymbol{\mu}_{\phi}(\boldsymbol{\theta}_1) - \tilde{\boldsymbol{\mu}}_{\phi}(\xi)) \quad (52)$$

or

$$D(p_{\mathbf{u};\boldsymbol{\theta}_0}||p_{\mathbf{u};\boldsymbol{\theta}_1}) \approx -(\boldsymbol{\mu}_\phi(\boldsymbol{\theta}_1) - \boldsymbol{\mu}_\phi(\boldsymbol{\theta}_0))^T \mathbf{R}_\phi^{-1}(\tilde{\boldsymbol{\theta}}(\xi)) (\boldsymbol{\mu}_\phi(\boldsymbol{\theta}_0) - \tilde{\boldsymbol{\mu}}_\phi(\xi)), \quad (53)$$

$$D(p_{\mathbf{u};\boldsymbol{\theta}_1}||p_{\mathbf{u};\boldsymbol{\theta}_0}) \approx (\boldsymbol{\mu}_\phi(\boldsymbol{\theta}_1) - \boldsymbol{\mu}_\phi(\boldsymbol{\theta}_0))^T \mathbf{R}_\phi^{-1}(\tilde{\boldsymbol{\theta}}(\xi)) (\boldsymbol{\mu}_\phi(\boldsymbol{\theta}_1) - \tilde{\boldsymbol{\mu}}_\phi(\xi)). \quad (54)$$

With the Fisher information matrix for distributions (21) being characterized by [24]

$$\mathbf{F}(\boldsymbol{\theta}) = \mathbb{E}_{\mathbf{u};\boldsymbol{\theta}} \left[\left(\frac{\partial \ln p_{\mathbf{u}}(\mathbf{u}; \boldsymbol{\theta})}{\partial \boldsymbol{\theta}} \right)^T \frac{\partial \ln p_{\mathbf{u}}(\mathbf{u}; \boldsymbol{\theta})}{\partial \boldsymbol{\theta}} \right] = \left(\frac{\partial \boldsymbol{\mu}_\phi(\boldsymbol{\theta})}{\partial \boldsymbol{\theta}} \right)^T \mathbf{R}_\phi^{-1}(\boldsymbol{\theta}) \frac{\partial \boldsymbol{\mu}_\phi(\boldsymbol{\theta})}{\partial \boldsymbol{\theta}}, \quad (55)$$

applying forward (106) and backward (107) approximations to (51) and (52), one obtains

$$D(p_{\mathbf{u};\boldsymbol{\theta}_0}||p_{\mathbf{u};\boldsymbol{\theta}_1}) \approx (\boldsymbol{\theta}_1 - \boldsymbol{\theta}_0)^T \mathbf{F}(\tilde{\boldsymbol{\theta}}(\xi)) (\tilde{\boldsymbol{\theta}}(\xi) - \boldsymbol{\theta}_0), \quad (56)$$

$$D(p_{\mathbf{u};\boldsymbol{\theta}_1}||p_{\mathbf{u};\boldsymbol{\theta}_0}) \approx (\boldsymbol{\theta}_1 - \boldsymbol{\theta}_0)^T \mathbf{F}(\tilde{\boldsymbol{\theta}}(\xi)) (\boldsymbol{\theta}_1 - \tilde{\boldsymbol{\theta}}(\xi)). \quad (57)$$

These approximations are reminiscent of expressions found in the literature [44, p. 85-86]

$$D(p_{\mathbf{u};\boldsymbol{\theta}_0}||p_{\mathbf{u};\boldsymbol{\theta}_1}) \approx -\frac{1}{2}(\boldsymbol{\theta}_1 - \boldsymbol{\theta}_0)^T \mathbf{F}(\boldsymbol{\theta}_0) (\boldsymbol{\theta}_1 - \boldsymbol{\theta}_0) = \tilde{D}(p_{\mathbf{u};\boldsymbol{\theta}_0}||p_{\mathbf{u};\boldsymbol{\theta}_1}), \quad (58)$$

$$D(p_{\mathbf{u};\boldsymbol{\theta}_1}||p_{\mathbf{u};\boldsymbol{\theta}_0}) \approx \frac{1}{2}(\boldsymbol{\theta}_1 - \boldsymbol{\theta}_0)^T \mathbf{F}(\boldsymbol{\theta}_1) (\boldsymbol{\theta}_1 - \boldsymbol{\theta}_0) = \tilde{D}(p_{\mathbf{u};\boldsymbol{\theta}_1}||p_{\mathbf{u};\boldsymbol{\theta}_0}), \quad (59)$$

while having a flexible probabilistic linearization model $\tilde{\boldsymbol{\theta}}(\xi)$. Note that (58) and (59) are derived in [44] for the special case of a natural exponential family which features the restriction $\boldsymbol{\beta}(\boldsymbol{\theta}) = \boldsymbol{\theta}$. A potential disadvantage of the approximations (56) and (57) is that access to the Fisher information matrix (55) of the exponential family model $p_{\mathbf{u}}(\mathbf{u}; \tilde{\boldsymbol{\theta}}(\xi))$ is required.

D. Controlling the Statistical Complexity of the ALLR

While (38) and (40) enable running and analyzing a likelihood-based test such as the SPRT via (25) and (26) without access to the likelihood ratio (24), they do per se not solve the intractability of such a test with many sufficient statistics C (as is the case with general multivariate binary distributions). For such cases, replacing the true data model by an auxiliary model [24]

$$\tilde{p}_{\mathbf{u}}(\mathbf{u}; \boldsymbol{\theta}) = \exp \left(\tilde{\boldsymbol{\beta}}^T(\boldsymbol{\theta}) \tilde{\boldsymbol{\phi}}(\mathbf{u}) - \tilde{\lambda}(\boldsymbol{\theta}) + \tilde{\nu}(\mathbf{u}) \right), \quad (60)$$

allows to control the LLR complexity. In (60), $\tilde{\boldsymbol{\phi}}(\mathbf{u}): \mathcal{U} \rightarrow \mathbb{R}^{\tilde{C}}$ is a suitable subset ($\tilde{C} < C$) of the sufficient statistics in the original model (21), i.e., $\boldsymbol{\phi}(\mathbf{u}) = \left[\tilde{\boldsymbol{\phi}}^T(\mathbf{u}) \quad \boldsymbol{\phi}'^T(\mathbf{u}) \right]^T$ while mean

$$\boldsymbol{\mu}_{\tilde{\boldsymbol{\phi}}}(\boldsymbol{\theta}) = \mathbb{E}_{\mathbf{u};\boldsymbol{\theta}} \left[\tilde{\boldsymbol{\phi}}(\mathbf{u}) \right] \quad (61)$$

and covariance

$$\mathbf{R}_{\tilde{\phi}}(\boldsymbol{\theta}) = \mathbb{E}_{\mathbf{u}, \boldsymbol{\theta}} \left[(\tilde{\phi}(\mathbf{u}) - \boldsymbol{\mu}_{\tilde{\phi}}(\boldsymbol{\theta})) (\tilde{\phi}(\mathbf{u}) - \boldsymbol{\mu}_{\tilde{\phi}}(\boldsymbol{\theta}))^T \right] \quad (62)$$

are equivalent when formed with respect to (60) or (21). It can be shown that [24]

$$\mathbf{F}(\boldsymbol{\theta}) \succeq \tilde{\mathbf{F}}(\boldsymbol{\theta}), \quad (63)$$

where $\tilde{\mathbf{F}}(\boldsymbol{\theta})$ is the Fisher information matrix (55) under the auxiliary model (60). Due to the matrix inequality (63) and the quadratic form of (56) and (57), (60) provides a conservative modification of (38) and (40). In the following, when evaluating (53)–(57) for the hard-limited version of (4), we use an auxiliary model (60) with sufficient statistics [24]

$$\tilde{\phi}(\mathbf{z}) = \Phi \text{vec}(\mathbf{z}\mathbf{z}^T), \quad (64)$$

where $\Phi \in [0; 1]^{\tilde{C} \times (MK)^2}$ is an elimination matrix canceling the duplicate and constant statistics on $\mathbf{z}\mathbf{z}^T$. For the calculation of (25) and (26) with (64), we proceed as described in [45] and use the arc-sin law [46, p. 284] and results for the quadrivariate orthant probabilities [47].

V. ACCURACY OF THE LLR APPROXIMATION

A. Digital Data Model and Error Measures

To analyze the accuracy of (38) and (40), we consider a Gaussian model with $\theta \in \mathbb{R}$

$$p_{\mathbf{y}}(\mathbf{y}; \theta) = \frac{\exp\left(-\frac{1}{2}\mathbf{y}^T \mathbf{R}_{\mathbf{y}}^{-1}(\theta)\mathbf{y}\right)}{\sqrt{(2\pi)^K \det(\mathbf{R}_{\mathbf{y}}(\theta))}}. \quad (65)$$

Note, that by

$$\mathbf{y}^T \mathbf{R}_{\mathbf{y}}^{-1}(\theta)\mathbf{y} = \text{tr}(\mathbf{R}_{\mathbf{y}}^{-1}(\theta)\mathbf{y}\mathbf{y}^T) = \text{vec}(\mathbf{R}_{\mathbf{y}}^{-1}(\theta)) \text{vec}(\mathbf{y}\mathbf{y}^T), \quad (66)$$

the probability density (65) can be factorized along (21) by setting $\nu(\mathbf{y}) = 0$ and

$$\boldsymbol{\beta}(\theta) = -\frac{1}{2} \text{vec}(\mathbf{R}_{\mathbf{y}}^{-1}(\theta)), \quad (67)$$

$$\boldsymbol{\phi}(\mathbf{y}) = \text{vec}(\mathbf{y}\mathbf{y}^T), \quad (68)$$

$$\lambda(\theta) = \frac{1}{2} \ln \det(\mathbf{R}_{\mathbf{y}}(\theta)) + \frac{K}{2} \ln 2\pi. \quad (69)$$

Additionally, with (68), one obtains

$$\boldsymbol{\mu}_{\phi}(\theta) = \text{vec}(\mathbf{R}_{\mathbf{y}}(\theta)) \quad \text{and} \quad \mathbf{R}_{\phi}(\theta) = 2(\mathbf{R}_{\mathbf{y}}(\theta) \otimes \mathbf{R}_{\mathbf{y}}(\theta)). \quad (70)$$

The exact expected LLRs between two Gaussian distributions (65) are given by

$$\mu_0 = \frac{1}{2} \ln \frac{\det(\mathbf{R}_y(\theta_0))}{\det(\mathbf{R}_y(\theta_1))} + \frac{K}{2} - \frac{1}{2} \text{tr}(\mathbf{R}_y^{-1}(\theta_1) \mathbf{R}_y(\theta_0)), \quad (71)$$

$$\mu_1 = \frac{1}{2} \ln \frac{\det(\mathbf{R}_y(\theta_0))}{\det(\mathbf{R}_y(\theta_1))} - \frac{K}{2} + \frac{1}{2} \text{tr}(\mathbf{R}_y^{-1}(\theta_0) \mathbf{R}_y(\theta_1)). \quad (72)$$

Therefore, under the Gaussian distribution (65), we can evaluate the relative approximation errors

$$\tilde{\epsilon}_i(\xi) = \frac{|\tilde{\mu}_i(\xi)| - |\mu_i|}{|\mu_i|}, \quad i = 1, 2, \quad (73)$$

and compare them to (58) and (59) through the expression

$$\tilde{\epsilon}_i = \frac{\tilde{D}(p_{\mathbf{u};\theta_i} || p_{\mathbf{u};\theta_j}) - D(p_{\mathbf{u};\theta_i} || p_{\mathbf{u};\theta_j})}{D(p_{\mathbf{u};\theta_i} || p_{\mathbf{u};\theta_j})}, \quad i = 1, 2; i \neq j. \quad (74)$$

B. Application - Sampling Random Gaussian Processes

To connect the multivariate Gaussian model (65) to a practical sensing application, we assume that it models the digital data stream obtained by sampling (1) with $M = 1$ via an ideal A/D converter featuring ∞ -bit amplitude resolution. The continuous-time Gaussian random process $y(t) \in \mathbb{R}$ is assumed to be the superposition of a band-limited source signal $\check{s}(t) \in \mathbb{R}$ and white noise $\check{\eta}(t)$ after pre-processing with an ideal low-pass filter $h(t; B)$ of bandwidth $B = B_y$, i.e.,

$$y(t) = h(t; B_y) * (\check{s}(t) + \check{\eta}(t)). \quad (75)$$

The ideally band-limited source $\check{s}(t)$ features constant power spectral density $\Psi_s(\omega) = \Psi_s, \omega \in [-\Omega_s; \Omega_s]$ with $\Omega_s \leq \Omega_y$, and $\Psi_s(\omega) = 0$ elsewhere. Consequently, the source passes unaffected

$$s(t) = h(t; B_y) * \check{s}(t) = \check{s}(t). \quad (76)$$

The noise $\check{\eta}(t)$ has constant density $\Psi_\eta(\omega) = \Psi_\eta$ on $\omega \in [-\Omega_\eta; \Omega_\eta]$ with $\Omega_\eta \gg \Omega_y$. Consequently,

$$\eta(t) = h(t; B_y) * \check{\eta}(t) \neq \check{\eta}(t). \quad (77)$$

Note, that by the Wiener–Khinchin theorem the auto-correlation function of a band-limited random process $u(t)$ (bandwidth B_u or Ω_u) with constant power spectral density Ψ_u is

$$r_u(t) = \text{E}_u [u(\tau)u(\tau - t)] = \frac{1}{2\pi} \int_{-\Omega_u}^{\Omega_u} \Psi_u(\omega) e^{j\omega t} d\omega = \frac{\Psi_u \sin(2\pi B_u t)}{\pi t} = 2B_u \Psi_u \text{sinc}(2B_u t). \quad (78)$$

With the filter $h(t; B_y)$ including a gain-control factor $\frac{1}{\sqrt{2B_y\Psi_\eta}}$ and sampling K times at a rate $f_T = \frac{1}{T} = 2B_y$, the digital data covariance is

$$\mathbf{R}_y(\theta) = \mathbf{R}_s(\theta) + \mathbf{R}_\eta = \frac{\theta}{\kappa}\boldsymbol{\Sigma}(\kappa) + \mathbf{I}, \quad (79)$$

where the SNR is

$$\theta = \text{SNR} = \frac{\Psi_s}{\Psi_\eta}. \quad (80)$$

With a source oversampling factor of $\kappa = \frac{B_y}{B_s} \geq 1$ the source covariance matrix has entries

$$[\boldsymbol{\Sigma}(\kappa)]_{ij} = \text{sinc}\left(\frac{|i-j|}{\kappa}\right), \quad i, j = 1, \dots, K. \quad (81)$$

Note that, in contrast to the source covariance $\mathbf{R}_s(\theta)$, in (79) the noise covariance \mathbf{R}_η is the identity matrix (temporally white noise) irrespective of the oversampling κ as, through the relation $f_T = 2B_y = \kappa 2B_s$, the sampling rate f_T and the bandwidth B_y of the noise after pre-filtering are proportional. For illustration, Fig. 1 visualizes an exemplary sensing situation with $\kappa = 2$ and

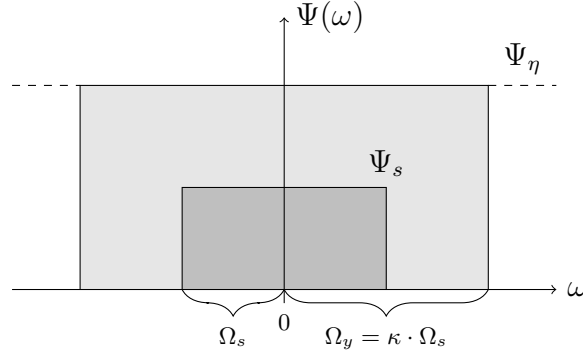


Fig. 1: Power Spectral Density and Bandwidth ($\kappa = 2$, SNR = -3.0 dB)

SNR = -3.0 dB in the frequency domain. Note, that we define (80) independently of $h(t; B_y)$ and κ to ensure that the design of the analog pre-processing does not affect the resulting SNR.

C. Results - Approximation Accuracy

Fig. 2a shows the relative errors (73) and (74) for a setting with $K = 10$, $\kappa = 2$, $\theta_0 = -20$ dB as a function of θ_1 . It can be observed that the error $|\tilde{\epsilon}_i|$ increases quickly with the distance $\theta_1 - \theta_0$ and beyond $\theta_1 = -10$ dB exceeds 27.1%. In contrast, for all SNR values, the error $|\epsilon_i(\frac{1}{2})|$ is not larger than 22.3%. Using (50) with $\rho = \frac{2}{3}$, the error $|\epsilon_i(\xi^*)|$ is below 2.6% over the entire depicted SNR range. Fig. 2b shows ξ^* resulting from (50) with $\rho = \frac{2}{3}$.

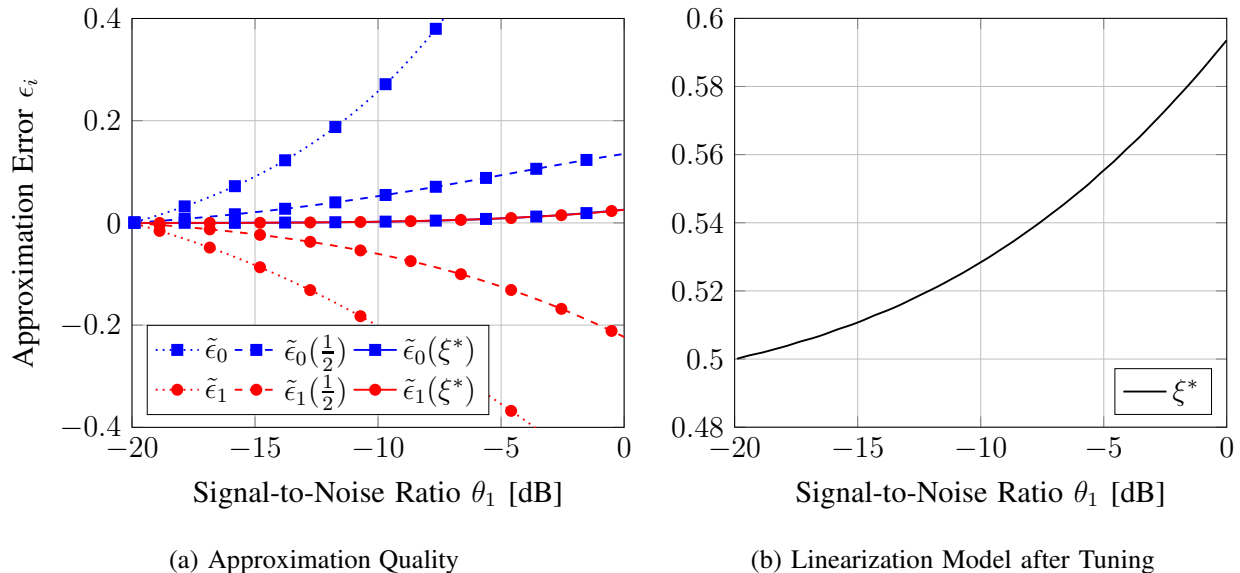


Fig. 2: ALLR - Approximation Quality and Tuning ($K = 10, \kappa = 2, \theta_0 = -20$ dB)

Note, that a typical sequential task is to detect small SNR changes from the digital measurements. To assess the quality of (40) in such a context, using the definition $\theta_0 = \bar{\theta} - \Delta_\theta$ and $\theta_1 = \bar{\theta} + \Delta_\theta$, in Fig. 3a we visualize the relative errors (73) and (74) for $\Delta_\theta = 1.5$ dB, $K = 10, \kappa = 2$, as a function of $\bar{\theta}$. The error $|\tilde{\epsilon}_i|$ exceeds 16.6% for $\bar{\theta} \geq -5$ dB. The relative error $|\epsilon_i(\frac{1}{2})|$ stays below 9.2% for all SNR values, while employing (50) with $\rho = \frac{2}{3}$ results in ξ^* shown in Fig. 3b and an error $|\epsilon_i(\xi^*)|$ smaller than 0.52%. In summary, the results for the exemplary model (65) show that (40) is of high quality, in particular if the statistical midpoint $\tilde{\theta}(\xi)$ is optimized.

VI. APPLICATION - BINARY RADIO SYSTEM DESIGN

The impact of results like (38) or (40) on technical systems is illustrated by exemplary applications in radio system engineering. To emphasize the significance of binary sensor and data processing technology for future wireless systems at large, we use a consumer-oriented cognitive sensing application with low complexity as the main focus and a safety-critical spectrum monitoring application with a distinct emphasis on high performance. For each application, we assume a particular analog front-end architecture when modeling the received radio signals (1).

A. Low-Cost Cognitive Radio Communication Systems

First, we consider a cognitive system for mobile radio communication. The task of the receive system is to monitor a certain part of the spectrum and to determine whether a primary transmitter

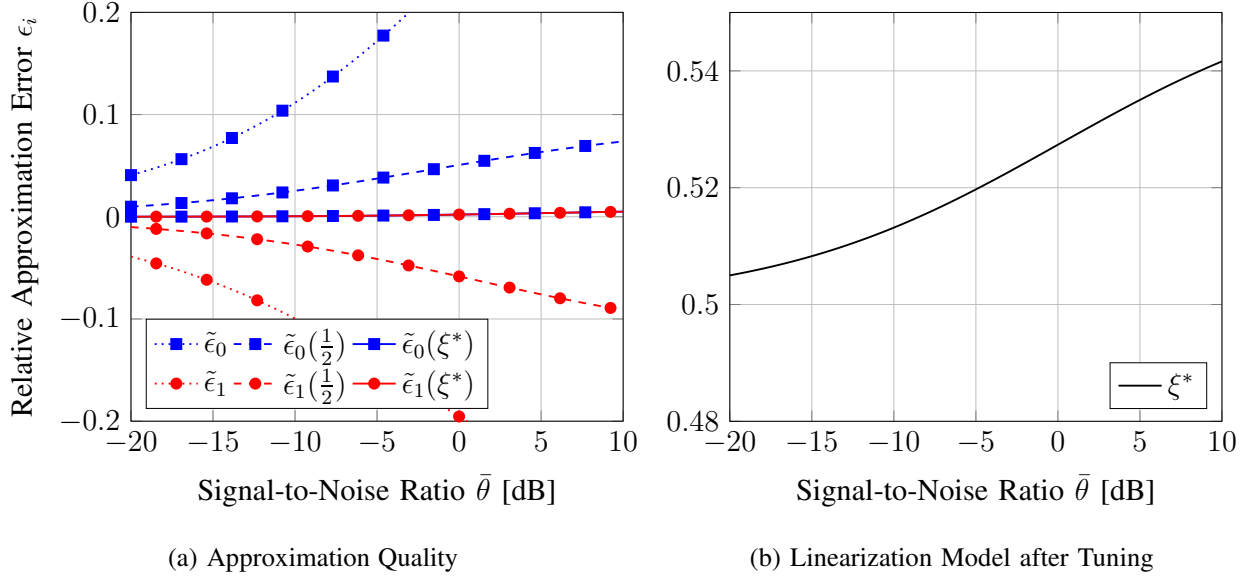


Fig. 3: ALLR - Approximation Quality and Tuning ($K = 10, \kappa = 2, \Delta\theta = 1.5$ dB)

is currently utilizing the radio channel. The basic scenario is, therefore, similar to the example considered in Sec. V. However, when modeling the analog output (1), it is important to take into account the precise front-end architecture. For cognitive radio, we assume a superheterodyne receiver as depicted in Fig. 4. The difficulty in modeling its analog outputs lies in the fact that

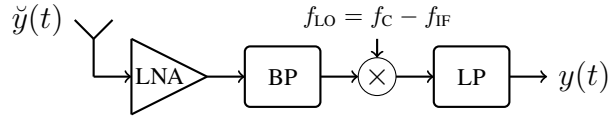


Fig. 4: Analog Sensor Front-End - Superheterodyne Wireless Receiver

the receiver does not demodulate with the carrier frequency f_C of the transmitter. The received signal is demodulated by a local oscillator with $f_{LO} = f_C - f_{IF}$, where $f_{IF} < f_C$ is an intermediate frequency (IF). As a consequence, sampling is performed on one real-valued analog output

$$y(t) = x_I(t)\sqrt{2}\cos(\omega_{IF}t) - x_Q(t)\sqrt{2}\sin(\omega_{IF}t) + \eta(t), \quad (82)$$

where $x_I(t)$ and $x_Q(t)$ are assumed two jointly independent zero-mean Gaussian processes of bandwidth B_s modeling the primary transmitter. The independent zero-mean Gaussian process $\eta(t)$ models sensor noise with bandwidth B_y . Sampling K times at a rate of $\frac{1}{T} = 2B_y$ and with an amplitude resolution of $b = \infty$ bits, one obtains zero-mean multivariate Gaussian data with

$$\mathbf{R}_y(\theta) = \frac{\theta}{\kappa} \Sigma(\kappa) \odot 2\mathbf{W} + \mathbf{I}, \quad \mathbf{R}_y(\theta) \in \mathbb{R}^{K \times K}, \quad (83)$$

where the parameter θ is the received SNR as defined in (80), $\Sigma(\kappa)$ the source covariance as defined in (81), and the matrix $\mathbf{W} \in \mathbb{R}^{K \times K}$ models the mixing effects at the intermediate frequency f_{IF} . For simplicity, we assume f_{IF} to be symmetric with respect to the bandwidth B_y of the low-pass (LP) filter, i.e., $f_{\text{IF}} = \frac{B_y}{2}$. Thus the entries of the mixing matrix are

$$\begin{aligned} [\mathbf{W}]_{ij} &= \cos(\omega_{\text{IF}}T(i-1)) \cos(\omega_{\text{IF}}T(j-1)) + \sin(\omega_{\text{IF}}T(i-1)) \sin(\omega_{\text{IF}}T(j-1)) \\ &= \cos\left(\frac{\pi}{2}(i-1)\right) \cos\left(\frac{\pi}{2}(j-1)\right) + \sin\left(\frac{\pi}{2}(i-1)\right) \sin\left(\frac{\pi}{2}(j-1)\right). \end{aligned} \quad (84)$$

Fig. 5 visualizes the power spectral densities and signal bandwidths for a setting with superheterodyne front-end and $\kappa = 4$, $\text{SNR} = -3.0$ dB. For the considered superheterodyne receiver,

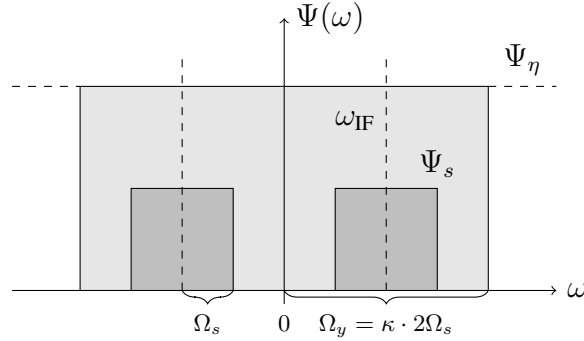


Fig. 5: Power Density and Signal Bandwidths (Superheterodyne, $\kappa = 4$, $\text{SNR} = -3.0$ dB)

the source bandwidth is $B_s \leq \frac{B_y}{2}$, such that $\kappa \geq 2$. For evaluation, we define relative efficiency

$$\chi_i = \frac{\tilde{\mu}_i(\xi^*)}{\mu_i}, \quad i = 1, 2, \quad (85)$$

to compare the binary sensing latency to the run-time with high-resolution sampling. Here we assume a binary receiver with $K = \kappa K_0$ such that the absolute observation time $T_o = KT$ of each block stays constant when increasing the temporal oversampling κ .

Fig. 6a shows (85) for a low SNR scenario with $\bar{\theta} = -15$ dB and $\Delta_\theta = 1.5$ dB. Without oversampling ($\kappa = 2$), binary sampling of the analog superheterodyne sensor signal (82) makes it impossible to perform the detection task. In such a case, the activity of the transmitter can only be detected by discriminating between two variance levels. The output of (6), however, is invariant to changes of the input scale. With oversampling, the presence of a band-limited source introduces correlation among the K samples (non-zero off-diagonal entries in (83)) which can be detected from the binary measurements. The ∞ -bit receiver does not benefit from oversampling

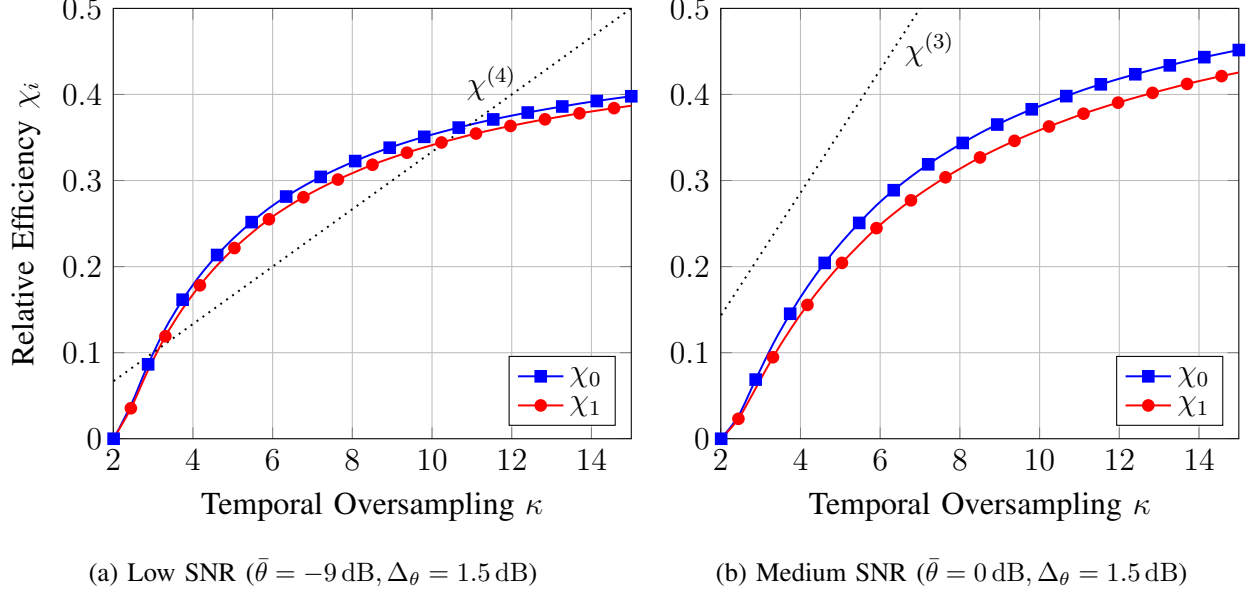


Fig. 6: Binary Cognitive Ratio (Superheterodyne, $M = 1, K_0 = 5$)

as the full information about the band-limited sources in (82) is already embedded in the digital measurement data obtained with $\kappa = 2$. Fig. 6b depicts the efficiency (85) at medium SNR ($\bar{\theta} = 0$ dB, $\Delta\theta = 1.5$ dB). Like for the low SNR case in Fig. 6a, oversampling decreases the detection latency. Fig. 6a and Fig. 6b show that, in general, a binary wireless receiver is suitable for cognitive radio. However, oversampling of the source signal is required and a larger latency needs to be accepted in return for the simplicity of the radio front-end and data structure.

For a quantitative perspective on complexity, we define the average sampling cost (ASC)

$$\text{ASC}^{(b)}(M, K; \boldsymbol{\theta}) = \text{SC}^{(b)}(M, K) \cdot \text{ASN}^{(b)}(\boldsymbol{\theta}). \quad (86)$$

A binary receiver outperforms a b -bit system in terms of A/D comparator operations when

$$\frac{\text{ASC}^{(1)}(M, K; \boldsymbol{\theta})}{\text{ASC}^{(b)}(M, K; \boldsymbol{\theta})} < 1. \quad (87)$$

For a cognitive radio system with the front-end depicted in Fig. 4, inequality (87) is fulfilled if

$$\frac{\text{SC}^{(1)}(M, \kappa K_0) \text{ASN}^{(1)}(\boldsymbol{\theta})}{\text{SC}^{(b)}(M, 2K_0) \text{ASN}^{(\infty)}(\boldsymbol{\theta})} < 1, \quad (88)$$

such that a 1-bit radio receiver which exceeds the efficiency level

$$\chi^{(b)} = \frac{\kappa}{2(2^b - 1)} \quad (89)$$

is superior to a b -bit device. Fig. 6a demonstrates that a binary device, in terms of (86), outperforms receivers with 4 or more bits A/D resolution. Under the conservative benchmark (88), Fig. 6b indicates that a binary system might not be able to compete with a 3-bit receiver.

B. High-Performance GNSS Spectrum Monitoring Systems

As a second application, we consider GNSS spectrum monitoring. The task is to detect interference in the vicinity of a satellite radio receiver synchronizing critical infrastructure (e.g., financial markets with high-speed trading, supply point of an electrical network) or providing correction data to mobile GNSS receivers which have a strict reliability requirement on their real-time positioning solution (e.g., ground-based augmentation system at an airport). In case the interference on the GNSS band exceeds a certain power level, the monitor issues a warning to the GNSS receiver which initiates measures to suppress the interference or reports a temporary malfunction. In contrast to the cognitive receiver in Sec. VI-A, for GNSS monitoring we assume

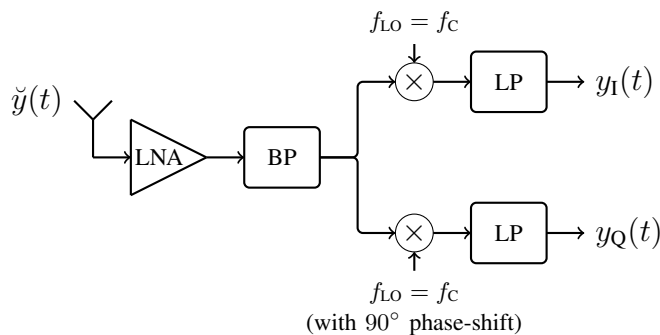


Fig. 7: Homodyne Analog Sensor Front-End

that the receiver features multiple antennas with a homodyne front-end as depicted in Fig. 7. Homodyne front-ends demodulate the received signal within two real-valued channels (in-phase and quadrature) at carrier frequency f_c , where the quadrature oscillator features a phase-shift of 90° relative to the in-phase demodulator. In the signal processing and communication engineering literature, the two real-valued outputs in Fig. 7 are usually summarized in one complex-valued variable. Note, that this is a mathematical convention which serves compactness. The information embedded in the two signals and thus the achievable performance does not change when switching between real-valued and complex-valued notation. In fact, complex-valued Gaussian models are usually limited to both outputs being uncorrelated and of equivalent variance. Removing these limitations within a complex-valued framework requires additional effort with respect to

notation, see e.g., [48]. A real-valued characterization adjusted to the physical signal acquisition chain does not face such restrictions and allows analyzing unconventional front-ends [15]. With a superheterodyne front-end layout like in Fig. 4 and ∞ -bit A/D conversion, one can obtain the digital equivalents of the two analog outputs in Fig. 7 through digital processing. With low-resolution sampling, however, this is not possible. When analyzing homodyne front-ends, we stay in a real-valued notation, such that it is clear which sensor system forms the basis for the model (4) before the quantizer (6). Consequently, we denote the analog outputs (1) as $\mathbf{y}(t) = [\mathbf{y}_I^T(t) \ \mathbf{y}_Q^T(t)]^T$, where $\mathbf{y}_I(t) \in \mathbb{R}^{M_A}$ and $\mathbf{y}_Q(t) \in \mathbb{R}^{M_A}$ summarize the analog in-phase and quadrature outputs of the $M_A = \frac{M}{2}$ receivers. The analog outputs have the signal structure

$$\mathbf{y}(t) = \theta \mathbf{A} \mathbf{x}(t) + \boldsymbol{\eta}(t), \quad (90)$$

where the independent zero-mean random Gaussian processes $\mathbf{x}(t) = [x_I(t) \ x_Q(t)]^T$ model a wireless interferer with bandwidth $B_s = B_y$ received with a SNR θ . Under the assumption that the bandwidth B_y of the receivers is narrow in comparison to f_C and the M_A sensors are placed as a uniform linear array (ULA) with an element-wise distance of half the carrier wavelength, the response of the antenna array can be characterized by the array steering matrix $\mathbf{A} = [\mathbf{A}_I^T \ \mathbf{A}_Q^T]^T$, where the steering sub-matrices $\mathbf{A}_I, \mathbf{A}_Q \in \mathbb{R}^{M_A \times 2}$ are [45]

$$\mathbf{A}_I = \begin{bmatrix} \cos(0) & \sin(0) \\ \cos(\pi \sin(\varphi)) & \sin(\pi \sin(\varphi)) \\ \vdots & \vdots \\ \cos((M_A - 1)\pi \sin(\varphi)) & \sin((M_A - 1)\pi \sin(\varphi)) \end{bmatrix} \quad (91)$$

and

$$\mathbf{A}_Q = \begin{bmatrix} -\sin(0) & \cos(0) \\ -\sin(\pi \sin(\varphi)) & \cos(\pi \sin(\varphi)) \\ \vdots & \vdots \\ -\sin((M_A - 1)\pi \sin(\varphi)) & \cos((M_A - 1)\pi \sin(\varphi)) \end{bmatrix}, \quad (92)$$

while φ denotes the angle under which the source $\mathbf{x}(t)$ arrives. Assuming that the sampling rate is now given by the relation $f_T = \kappa 2B_y$, for a wireless array receiver with an ideal ∞ -bit A/D conversion process one obtains zero-mean multivariate Gaussian data (4) with covariance

$$\mathbf{R}_y(\theta) = (\theta \mathbf{A} \mathbf{A}^T + \mathbf{I}) \otimes \boldsymbol{\Sigma}(\kappa), \quad \mathbf{R}_y(\theta) \in \mathbb{R}^{MK \times MK}. \quad (93)$$

In this case, the noise is not necessarily temporally white as the sampling rate can be misaligned (in the sense of the sampling theorem) with the bandwidth of the analog pre-filter, i.e., $f_T > 2B_y$.

Fig. 8 shows the relative performance measure (85) where the GNSS spectrum is monitored by a binary array with $\bar{\theta} = -15$ dB SNR and $\Delta_\theta = 3$ dB. No temporal oversampling is performed, i.e., $\kappa = 1$. It can be observed that the efficiency of the binary array, in comparison to an ideal system, increases with the number of antennas. For the case of an array with homodyne

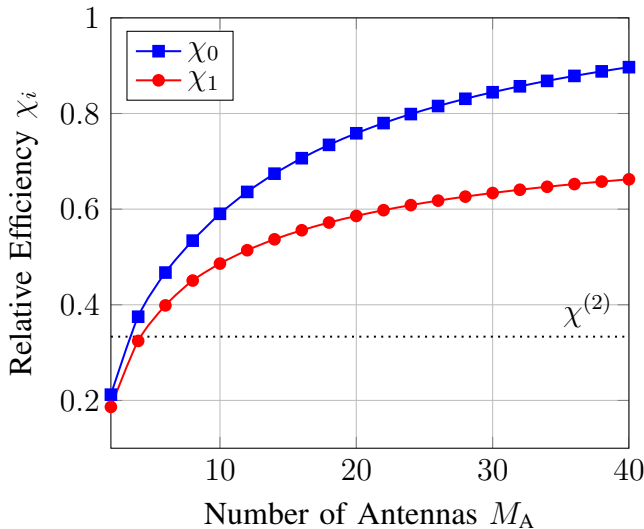


Fig. 8: Binary GNSS Monitoring (Homodyne, $\varphi = 15^\circ$, $\kappa = 1$, $K_0 = 1$, $\bar{\theta} = -15$ dB, $\Delta_\theta = 3$ dB)

front-ends, the inequality (87) holds when

$$\frac{\text{SC}^{(1)}(M, \kappa K_0) \text{ASN}^{(1)}(\boldsymbol{\theta})}{\text{SC}^{(b)}(M, K_0) \text{ASN}^{(\infty)}(\boldsymbol{\theta})} < 1. \quad (94)$$

Therefore, to outperform a b -bit homodyne array concerning the A/D cost measure (86), a binary system with the same number of radio antennas needs to exceed the efficiency level

$$\chi^{(b)} = \frac{\kappa}{2^b - 1}. \quad (95)$$

The results in Fig. 8 show that binary arrays with more than four homodyne antennas outperform 2-bit systems regarding digitization complexity when performing GNSS spectrum monitoring. To assess how many additional binary radio sensors are required to outperform an array receiver with an ideal ∞ -bit digitization process and m wireless sensors, we define the relative efficiency

$$\chi_{i,m} = \frac{\tilde{\mu}_i(\xi^*)}{\mu_i|_{M_A=m}}. \quad (96)$$

This measure is depicted in Fig. 9, where we use two ∞ -bit ULAs ($M_A = 4$ and $M_A = 16$) as performance benchmark. A binary array system with $M_A = 8$ antennas provides the same processing latency as a ∞ -bit A/D resolution system with $M_A = 4$ sensors. To outperform an ideal system with $M_A = 16$, a binary array with $M_A = 40$ sensors is required.

By using that (87) holds in the examined scenario if

$$\frac{\text{SC}^{(1)}(2M_A, \kappa K_0) \text{ASN}^{(1)}(\boldsymbol{\theta})}{\text{SC}^{(b)}(2m, K_0) \text{ASN}^{(\infty)}(\boldsymbol{\theta})} < 1, \quad (97)$$

Fig. 9 shows that both binary arrays ($M_A = 4$ and $M_A = 16$) significantly outperform

$$\chi^{(b,m)} = \frac{M_A}{m} \frac{\kappa}{(2^b - 1)} \quad (98)$$

evaluated for $b = 2$. Note that using (94) and (97) involves underestimating the ASN of a 2-bit

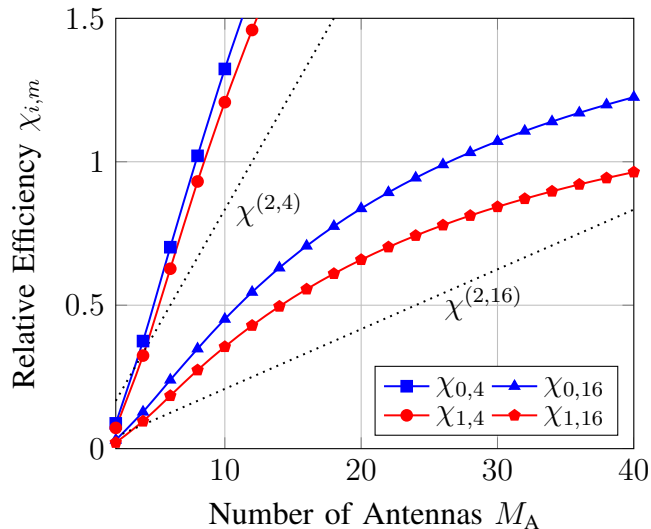


Fig. 9: Binary GNSS Monitoring (Homodyne, $\varphi = 5^\circ$, $\kappa = 1$, $K_0 = 1$, $\bar{\theta} = -15$ dB, $\Delta_\theta = 3$ dB) system by the ASN of a ∞ -bit receiver such that (95) and (98) form conservative thresholds.

VII. APPLICATION - LOW-LATENCY BINARY PROCESSING

As a final step, we investigate the accuracy of our latency analysis via (53) and (54) by Monte-Carlo simulations of the binary radio systems considered in Sec. VI. To this end, we optimize the ALLR with (50), run the ASPRT according to (43) and compare the empirical ASN with the analytic version obtained by (53) and (54). For the simulation, we run the sequential decision-making 10 000 times with independent observations and calculate the empirical ASN and error rate. The error rate which determines (14) and (15) is set to $\alpha_0 = \alpha_1 = 0.001$ for all experiments.

A. Low-Latency Decision-Making for Binary Cognitive Radio

For the cognitive radio setup with superheterodyne front-end (see Sec. VI-A), the simulation scenario is $M = 1, K_0 = 5, \kappa = \sqrt{35}$ with the hypotheses centered at a distance of $\Delta_\theta = 1.5$ dB around $\bar{\theta} = -9$ dB. Table I shows a comparison between the analytic and the empirical receiver operating characteristics of the ASPRT. The ∞ -bit digitization case, where we employ the exact LLR (24) and the Gaussian formulas (71) and (72), is given for comparison in Table II. The

Receiver Operating Characteristics					Receiver Operating Characteristics				
\mathcal{H}_i	α_i (the.)	α_i (sim.)	ASN_i (the.)	ASN_i (sim.)	\mathcal{H}_i	α_i (the.)	α_i (sim.)	ASN_i (the.)	ASN_i (sim.)
\mathcal{H}_0	0.0010	0.0010	1361.67	1367.38	\mathcal{H}_0	0.0010	0.0011	365.15	368.71
\mathcal{H}_1	0.0010	0.0007	1351.21	1373.34	\mathcal{H}_1	0.0010	0.0006	344.83	351.14

TABLE I: Binary Cognitive Radio

TABLE II: Ideal Cognitive Radio

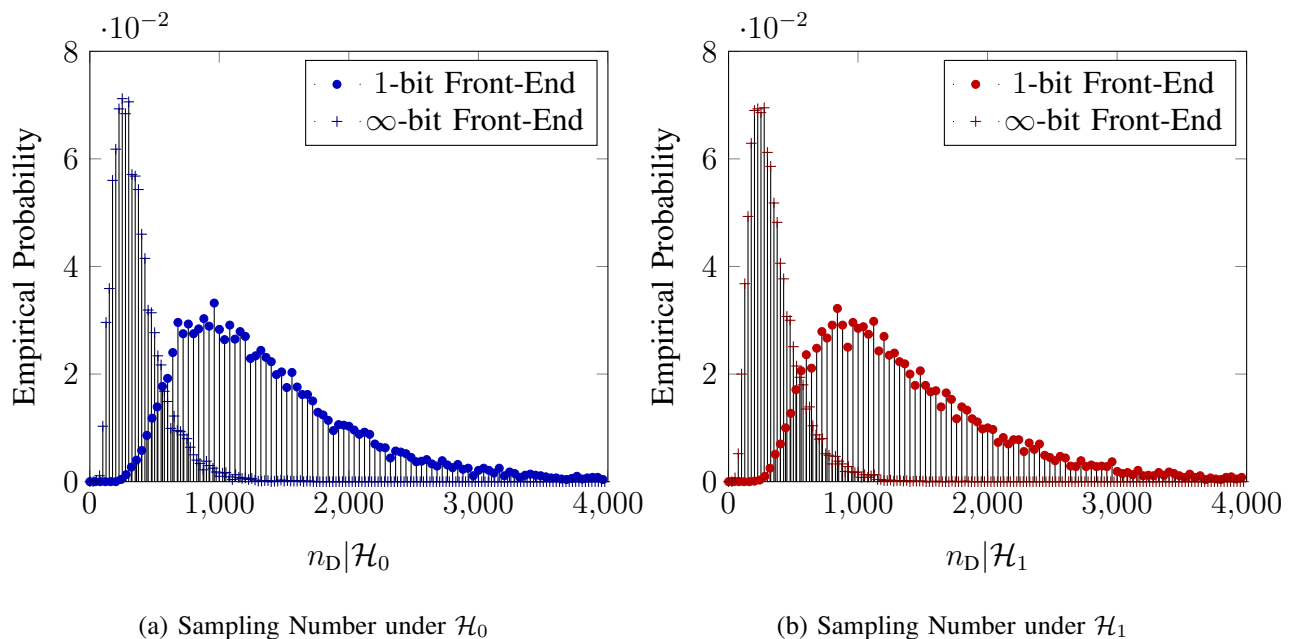


Fig. 10: Cognitive Radio (Superheterodyne, $M = 1, K_0 = 5, \kappa = 6, \bar{\theta} = -9$ dB, $\Delta_\theta = 1.5$ dB)

empirical evaluation of both sequential tests shows a good correspondence with the analytic results. For further illustration, the empirical distribution of the sampling number n_D under both hypotheses and digitization approaches is depicted in Fig. 10a and Fig. 10b. The results corroborate that a binary cognitive receiver is able to reliably sense the activity of a weak primary

user through temporal oversampling. As predicted by the analysis in Fig. 6a, the binary system requires significantly more samples than the ideal receiver to obtain the specified error level.

B. Low-Latency Decision-Making for Binary GNSS Monitoring

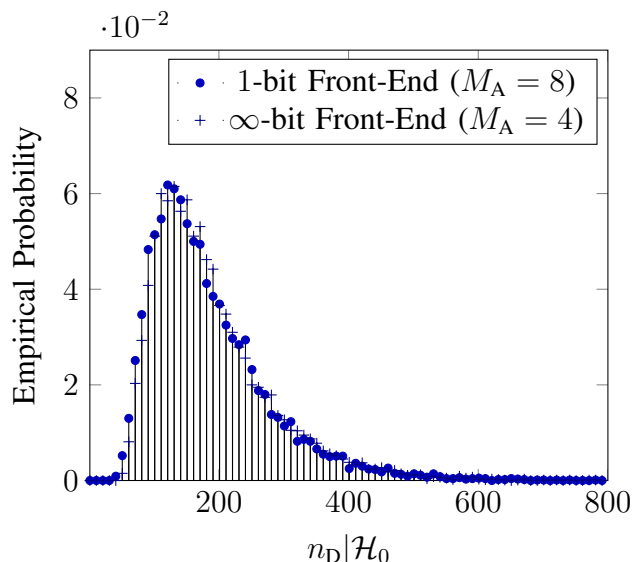
For a second set of simulations, we consider a ULA with $M_A = 8$ homodyne front-ends as analyzed in Sec. VI-B. The direction-of-arrival is $\varphi = 5^\circ$ and the sampling configuration $\kappa = 1, K_0 = 1$. The interference detection is performed by centering the two hypotheses around $\bar{\theta} = -15$ dB at a distance of $\Delta_\theta = 3$ dB. For comparison an ∞ -bit array system with half the amount of wireless sensors ($M_A = 4$) is used. Table III and Table IV show the obtained results. It can be observed that the empirical results match the analytic assessments. Fig. 11a and Fig. 11b

Receiver Operating Characteristics				
\mathcal{H}_i	α_i (the.)	α_i (sim.)	ASN $_i$ (the.)	ASN $_i$ (sim.)
\mathcal{H}_0	0.0010	0.0002	179.31	183.48
\mathcal{H}_1	0.0010	0.0010	162.20	168.09

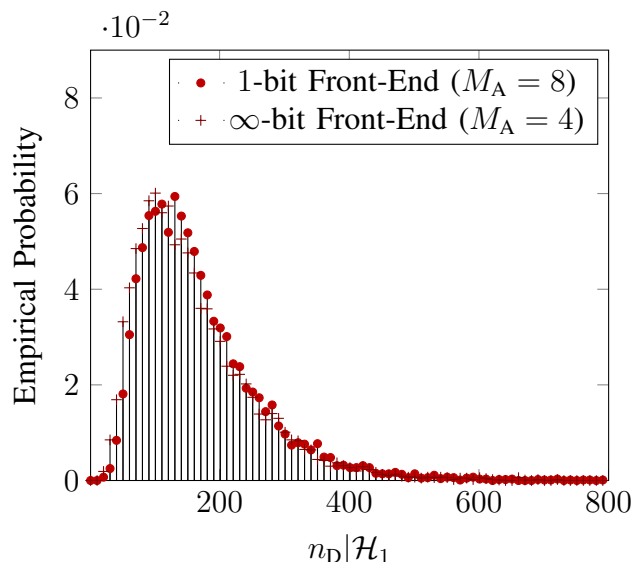
Receiver Operating Characteristics				
\mathcal{H}_i	α_i (the.)	α_i (sim.)	ASN $_i$ (the.)	ASN $_i$ (sim.)
\mathcal{H}_0	0.0010	0.0007	182.92	184.48
\mathcal{H}_1	0.0010	0.0014	150.99	159.43

TABLE III: Binary Monitoring ($M_A = 8$)

TABLE IV: Ideal Monitoring ($M_A = 4$)



(a) Sampling Number under \mathcal{H}_0



(b) Sampling Number under \mathcal{H}_1

Fig. 11: GNSS Monitoring (Homodyne, $\varphi = 5^\circ, \kappa = 1, K_0 = 1, \bar{\theta} = -15$ dB, $\Delta_\theta = 3$ dB)

show the empirical distribution of the sample number for both systems and hypotheses and confirm that double the amount of binary sensors can be sufficient to obtain a sensing apparatus equivalent to a ideal system with ∞ -bit A/D resolution. Note that (98) shows that the considered binary array ($M_A = 8$) provides this excellent performance at less than 66 % of the digitization cost than any other system with $M_A = 4$ and a higher A/D resolution. Nevertheless, it requires more space which is an aspect not reflected in our definition of digitization complexity (8).

VIII. CONCLUSION

We have discussed sequential detection with measurements from binary radio systems. Considering statistical tests in the exponential family, we circumvent the intractable distribution model arising when hard-limiting multivariate Gaussian data. We have derived approximations for the log-likelihood ratio and the Kullback–Leibler divergence, valid for any exponential family distribution. The expressions have the advantage that they can be adapted to the testing scenario and, therefore, provide stronger approximations than fixed methods. We applied these analytic results to the system design specification of wireless systems with binary digitization. The results show that radio systems with low-complexity front-ends are capable of performing challenging low-latency detection tasks. In particular, using a larger number of binary sensors shows to be a favorable approach concerning detection latency and digitization resources. Finally, we have demonstrated that our analysis matches the empirical behavior of sequential detectors operating based on binary radio data streams. In summary, our discussion provides a versatile framework for sequential tests with hardware-aware probabilistic modeling of sensor data streams and the rule of thumb that for a favorable complexity-latency trade-off in sensing architectures one reduces the amplitude resolution to a single bit and doubles the number of sensor devices.

APPENDIX

For $f : \mathbb{R} \rightarrow \mathbb{R}$, infinitely differentiable at $\hat{u} \in \mathbb{R}$, with $\Delta \in \mathbb{R}, \Delta \geq 0$, by the Taylor series

$$f(\hat{u} + \Delta) = \sum_{i=0}^{\infty} \frac{\Delta^i}{i!} \frac{\partial^i f(\hat{u})}{\partial u^i} \quad \text{and} \quad f(\hat{u} - \Delta) = \sum_{i=0}^{\infty} (-1)^i \frac{\Delta^i}{i!} \frac{\partial^i f(\hat{u})}{\partial u^i}. \quad (99)$$

A forward finite difference approximation at \hat{u} results in

$$f(\hat{u} + \Delta) - f(\hat{u}) \approx \frac{\partial f(\hat{u})}{\partial u} \Delta. \quad (100)$$

A backward finite difference approximation at \hat{u} results in

$$f(\hat{u}) - f(\hat{u} - \Delta) \approx \frac{\partial f(\hat{u})}{\partial u} \Delta. \quad (101)$$

Defining $\Delta_a, \Delta_b \in \mathbb{R}$ where $\Delta_a, \Delta_b \geq 0$, an alternative approximation at \hat{u} is

$$f(\hat{u} + \Delta_a) - f(\hat{u} - \Delta_b) \approx \frac{\partial f(\hat{u})}{\partial u} (\Delta_a + \Delta_b). \quad (102)$$

Defining $u_1 \geq u_0$, with the forward approximation (100)

$$f(u_1) - f(u_0) \approx \frac{\partial f(u_0)}{\partial u} (u_1 - u_0), \quad (103)$$

and with the backward approximation (101)

$$f(u_1) - f(u_0) \approx \frac{\partial f(u_1)}{\partial u} (u_1 - u_0). \quad (104)$$

Defining $\xi \in [0; 1]$ and $\hat{u} = \xi u_0 + (1 - \xi) u_1$, $\Delta_a = \xi(u_1 - u_0)$, $\Delta_b = (1 - \xi)(u_1 - u_0)$, with (102)

$$f(u_1) - f(u_0) \approx \frac{\partial f(\xi u_0 + (1 - \xi) u_1)}{\partial u} (u_1 - u_0). \quad (105)$$

Extending (103) - (105) to multivariate functions $\mathbf{f} : \mathbb{R}^A \rightarrow \mathbb{R}^B$, one obtains

$$\mathbf{f}(\mathbf{u}_1) - \mathbf{f}(\mathbf{u}_0) \approx \frac{\partial \mathbf{f}(\mathbf{u}_0)}{\partial \mathbf{u}} (\mathbf{u}_1 - \mathbf{u}_0), \quad (106)$$

$$\mathbf{f}(\mathbf{u}_1) - \mathbf{f}(\mathbf{u}_0) \approx \frac{\partial \mathbf{f}(\mathbf{u}_1)}{\partial \mathbf{u}} (\mathbf{u}_1 - \mathbf{u}_0), \quad (107)$$

$$\mathbf{f}(\mathbf{u}_1) - \mathbf{f}(\mathbf{u}_0) \approx \frac{\partial \mathbf{f}(\xi \mathbf{u}_0 + (1 - \xi) \mathbf{u}_1)}{\partial \mathbf{u}} (\mathbf{u}_1 - \mathbf{u}_0). \quad (108)$$

REFERENCES

- [1] B. Murmann. ADC performance survey 1997-2018. [Online]. Available: <http://web.stanford.edu/%7Emurmann/adcsurvey.html>
- [2] M. S. Stein, "Performance analysis for time-of-arrival estimation with oversampled low-complexity 1-bit A/D conversion," in *IEEE Int. Conference on Acoustics, Speech and Signal Processing (ICASSP)*, Mar. 2017, pp. 4491–4495.
- [3] M. T. Ivrlac and J. A. Nossek, "Challenges in coding for quantized MIMO systems," in *IEEE Int. Symposium on Information Theory*, July 2006, pp. 2114–2118.
- [4] O. Dabeer, J. Singh, and U. Madhow, "On the limits of communication performance with one-bit analog-to-digital conversion," in *IEEE Workshop on Signal Processing Advances in Wireless Communications*, July 2006, pp. 1–5.
- [5] A. Mezghani and J. A. Nossek, "On ultra-wideband MIMO systems with 1-bit quantized outputs: Performance analysis and input optimization," in *IEEE Int. Symposium on Information Theory*, June 2007, pp. 1286–1289.
- [6] J. Mo and R. W. Heath, "Capacity analysis of one-bit quantized MIMO systems with transmitter channel state information," *IEEE Trans. Signal Process.*, vol. 63, no. 20, pp. 5498–5512, Oct. 2015.
- [7] S. Jacobsson, G. Durisi, M. Coldrey, U. Gustavsson, and C. Studer, "One-bit massive MIMO: Channel estimation and high-order modulations," in *IEEE Int. Conference on Communication Workshop (ICCW)*, June 2015, pp. 1304–1309.

- [8] C. Mollén, J. Choi, E. G. Larsson, and R. W. Heath, “Uplink performance of wideband massive MIMO with one-bit ADCs,” *IEEE Trans. Wireless Commun.*, vol. 16, no. 1, pp. 87–100, Jan. 2017.
- [9] I. Daubechies and R. DeVore, “Approximating a bandlimited function using very coarsely quantized data: A family of stable sigma-delta modulators of arbitrary order,” *Ann. Math.*, vol. 158, no. 2, pp. 679–710, 2003.
- [10] U. S. Kamilov, A. Bourquard, A. Amini, and M. Unser, “One-bit measurements with adaptive thresholds,” *IEEE Signal Process. Lett.*, vol. 19, no. 10, pp. 607–610, Oct. 2012.
- [11] P. T. Boufounos, L. Jacques, F. Krahmer, and R. Saab, *Quantization and Compressive Sensing*. Cham: Springer International Publishing, 2015, pp. 193–237.
- [12] A. Host-Madsen and P. Handel, “Effects of sampling and quantization on single-tone frequency estimation,” *IEEE Trans. Signal Process.*, vol. 48, no. 3, pp. 650–662, Mar. 2000.
- [13] A. Ribeiro and G. B. Giannakis, “Bandwidth-constrained distributed estimation for wireless sensor networks - Part I: Gaussian case,” *IEEE Trans. Signal Process.*, vol. 54, no. 3, pp. 1131–1143, Mar. 2006.
- [14] A. Mezghani, F. Antreich, and J. A. Nossek, “Multiple parameter estimation with quantized channel output,” in *Int. ITG Workshop on Smart Antennas (WSA)*, Feb. 2010, pp. 143–150.
- [15] M. Stein, S. Theiler, and J. A. Nossek, “Overdemodulation for high-performance receivers with low-resolution ADC,” *IEEE Wireless Commun. Lett.*, vol. 4, no. 2, pp. 169–172, Apr. 2015.
- [16] Y. Li, C. Tao, G. Seco-Granados, A. Mezghani, A. L. Swindlehurst, and L. Liu, “Channel estimation and performance analysis of one-bit massive MIMO systems,” *IEEE Trans. Signal Process.*, vol. 65, no. 15, pp. 4075–4089, Aug. 2017.
- [17] A. Mezghani and A. L. Swindlehurst, “Blind estimation of sparse broadband massive MIMO channels with ideal and one-bit ADCs,” *IEEE Trans. Signal Process.*, vol. 66, no. 11, pp. 2972–2983, June 2018.
- [18] P. Willett and P. F. Swaszek, “On the performance degradation from one-bit quantized detection,” *IEEE Trans. Inf. Theory*, vol. 41, no. 6, pp. 1997–2003, Nov. 1995.
- [19] D. Ciuonzo, G. Papa, G. Romano, P. Salvo Rossi, and P. Willett, “One-bit decentralized detection with a Rao test for multisensor fusion,” *IEEE Signal Process. Lett.*, vol. 20, no. 9, pp. 861–864, Sep. 2013.
- [20] M. S. Stein, “Asymptotic signal detection rates with 1-bit array measurements,” in *IEEE Int. Conference on Acoustics, Speech and Signal Processing (ICASSP)*, Apr. 2018, pp. 4534–4538.
- [21] S. Tantaratana and J. Thomas, “Quantization for sequential signal detection,” *IEEE Trans. Commun.*, vol. 25, no. 7, pp. 696–703, July 1977.
- [22] A. Wald, “Sequential tests of statistical hypotheses,” *Ann. Math. Statist.*, vol. 16, no. 2, pp. 117–186, 1945.
- [23] M. Fauß and A. M. Zoubir, “A linear programming approach to sequential hypothesis testing,” *Sequential Analysis*, vol. 34, no. 2, pp. 235–263, 2015.
- [24] M. S. Stein, J. A. Nossek, and K. Barbé, “Fisher information lower bounds with applications in hardware-aware nonlinear signal processing,” 2015. [Online]. Available: <http://arxiv.org/abs/1512.03473>
- [25] E. Axell, G. Leus, E. G. Larsson, and H. V. Poor, “Spectrum sensing for cognitive radio: State-of-the-art and recent advances,” *IEEE Signal Process. Mag.*, vol. 29, no. 3, pp. 101–116, May 2012.
- [26] A. Broumandan, A. Jafarnia-Jahromi, S. Daneshmand, and G. Lachapelle, “Overview of spatial processing approaches for GNSS structural interference detection and mitigation,” *Proc. IEEE*, vol. 104, no. 6, pp. 1246–1257, June 2016.
- [27] R. T. Ioannides, T. Pany, and G. Gibbons, “Known vulnerabilities of global navigation satellite systems, status, and potential mitigation techniques,” *Proc. IEEE*, vol. 104, no. 6, pp. 1174–1194, June 2016.
- [28] H. R. Hashemi and I. B. Rhodes, “Decentralized sequential detection,” *IEEE Trans. Inf. Theory*, vol. 35, no. 3, pp. 509–520, May 1989.

- [29] V. V. Veeravalli, T. Basar, and H. V. Poor, "Decentralized sequential detection with a fusion center performing the sequential test," *IEEE Trans. Inf. Theory*, vol. 39, no. 2, pp. 433–442, Mar. 1993.
- [30] A. M. Hussain, "Multisensor distributed sequential detection," *IEEE Trans. Aerosp. Electron. Syst.*, vol. 30, no. 3, pp. 698–708, July 1994.
- [31] Y. Mei, "Asymptotic optimality theory for decentralized sequential hypothesis testing in sensor networks," *IEEE Trans. Inf. Theory*, vol. 54, no. 5, pp. 2072–2089, May 2008.
- [32] Y. Yilmaz, G. V. Moustakides, and X. Wang, "Cooperative sequential spectrum sensing based on level-triggered sampling," *IEEE Trans. Signal Process.*, vol. 60, no. 9, pp. 4509–4524, Sep. 2012.
- [33] S. Chaudhari, J. Lundn, and V. Koivunen, "Effects of quantization and channel errors on sequential detection in cognitive radios," in *Annual Conference on Information Sciences and Systems (CISS)*, Mar. 2012, pp. 1–6.
- [34] Y. Wang and Y. Mei, "Quantization effect on the log-likelihood ratio and its application to decentralized sequential detection," *IEEE Trans. Signal Process.*, vol. 61, no. 6, pp. 1536–1543, Mar. 2013.
- [35] R. S. Blum, "Quantization in multisensor random signal detection," *IEEE Trans. Inf. Theory*, vol. 41, no. 1, pp. 204–215, Jan. 1995.
- [36] X. Nguyen, M. J. Wainwright, and M. I. Jordan, "On optimal quantization rules for sequential decision problems," in *IEEE Int. Symposium on Information Theory*, July 2006, pp. 2652–2656.
- [37] D. Teng and E. Ertin, "Optimal quantization of likelihood for low complexity sequential testing," in *IEEE Global Conference on Signal and Information Processing*, Dec. 2013, pp. 675–678.
- [38] J. Choi, J. Mo, and R. W. Heath, "Near maximum-likelihood detector and channel estimator for uplink multiuser massive MIMO systems with one-bit ADCs," *IEEE Trans. Commun.*, vol. 64, no. 5, pp. 2005–2018, May 2016.
- [39] S. Hong and N. Lee, "Soft-output detector for uplink MU-MIMO systems with one-bit ADCs," *IEEE Commun. Lett.*, vol. 22, no. 5, pp. 930–933, May 2018.
- [40] M. S. Stein, S. Bar, J. A. Nossek, and J. Tabrikian, "Performance analysis for channel estimation with 1-bit ADC and unknown quantization threshold," *IEEE Trans. Signal Process.*, vol. 66, no. 10, pp. 2557–2571, May 2018.
- [41] B. Dai, S. Ding, and G. Wahba, "Multivariate Bernoulli distribution," *Bernoulli*, vol. 19, no. 4, pp. 1465–1483, 2013.
- [42] S. S. Gupta, "Probability integrals of multivariate normal and multivariate t^1 ," *Ann. Math. Statist.*, vol. 34, no. 3, pp. 792–828, 09 1963.
- [43] M. S. Stein and M. Fauß, "In a one-bit rush: Low-latency wireless spectrum monitoring with binary sensor arrays," in *IEEE Statistical Signal Processing Workshop (SSP)*, June 2018, pp. 223–227.
- [44] A. Tartakovsky, I. Nikiforov, and M. Basseville, *Sequential Analysis: Hypothesis Testing and Changepoint Detection*. Chapman & Hall, 2014.
- [45] M. Stein, K. Barbé, and J. A. Nossek, "DOA parameter estimation with 1-bit quantization - Bounds, methods and the exponential replacement," in *Int. ITG Workshop on Smart Antennas (WSA)*, Mar. 2016, pp. 1–6.
- [46] J. B. Thomas, *An introduction to statistical communication theory*. Wiley, 1969.
- [47] M. Sinn and K. Keller, "Covariances of zero crossings in Gaussian processes," *Theory of Probability & Its Applications*, vol. 55, no. 3, pp. 485–504, 2011.
- [48] P. J. Schreier and L. L. Scharf, *Statistical Signal Processing of Complex-Valued Data: The Theory of Improper and Noncircular Signals*. Cambridge University Press, 2010.